Cosmic structure, averaging and dark energy[1]

David L. Wiltshire

Department of Physics & Astronomy, University of Canterbury, Private Bag 4800, Christchurch 8140, New Zealand

Abstract. These lecture notes review the theoretical problems associated with coarse-graining the observed inhomogeneous structure of the universe at late epochs, of describing average cosmic evolution in the presence of growing inhomogeneity, and of relating average quantities to physical observables. In particular, a detailed discussion of the timescape scenario is presented. In this scenario, dark energy is realized as a misidentification of gravitational energy gradients which result from gradients in the kinetic energy of expansion of space, in the presence of density and spatial curvature gradients that grow large with the growth of structure. The phenomenology and observational tests of the timescape model are discussed in detail, with updated constraints from Planck satellite data. In addition, recent results on the variation of the Hubble expansion on $\lesssim 100\,h^{-1}$Mpc scales are discussed. The spherically averaged Hubble law is significantly more uniform in the rest frame of the Local Group of galaxies than in the conventional rest frame assumed for the Cosmic Microwave Background. This unexpected result supports a fundamental revision of the notion of the cosmic rest frame, consistent with the expectations of the timescape scenario.

Keywords: dark energy, theoretical cosmology, observational cosmology
PACS: 98.80.-k 98.80.Es 95.36.+x 98.80.Jk

1. INTRODUCTION

Present cosmological observations point to the need for a revolution in our physical understanding. On one hand we have a very successful phenomenological description of the universe based on the spatially homogeneous and isotropic Friedmann–Lemaître–Robertson–Walker (FLRW) geometry. However, this success comes at the price of the introduction of forms of mass–energy that have never been directly observed, and which constitute most of the stuff in the Universe: 27% in the form of clumped nonbaryonic dark matter, and 68% in the form of a smooth dark energy [1]. Unknowns of this magnitude demand that we carefully re-examine the assumptions of our physical models of the universe, and that we pay careful attention to all observations.

The universe was certainly homogeneous to a high degree at the epoch of last scattering, when the cosmic microwave background (CMB) radiation was laid down. However, at the present epoch the matter distribution displays a complex hierarchical structure with significant inhomogeneities up to scales of at least $100\,h^{-1}$Mpc, where h is the dimensionless parameter related to the Hubble constant by $H_0 = 100h\,\mathrm{km\,s^{-1}\,Mpc^{-1}}$. The present universe is dominated in volume by voids, with some 40% of the volume in voids of a characteristic diameter $\sim 30\,h^{-1}$Mpc [2]–[4] and populations of smaller minivoids [5]. Galaxy clusters are grouped in sheets that surround the voids, and filaments thread

[1] Based on 5 lectures at *15th Brazilian School on Cosmology and Gravitation*, Mangatariba, August 2012.

To appear in the Proceedings, edited by S. E. Perez Bergliaffa and M. Novello.

them, in a complex cosmic web [6].

A cosmological constant, Λ, as a source of dark energy might in itself not pose a great theoretical puzzle, were it not for the *cosmic coincidence problem*: why is the value of Λ such that the universe decelerates for much of its history and only begins to accelerate relatively recently? In addition, there is another cosmic coincidence, which some cosmologists view as a smoking gun: the onset of cosmic acceleration also coincides with the epoch in which the large nonlinear structures of the cosmic web begin to dominate, as the map of the time history of universe [7] clearly reveals.

The possibility that the phenomenon of dark energy is actually accounting for the average effects of inhomogeneous structures on the expansion history of the universe has led to an upsurge of interest in the averaging problem in cosmology. This is a foundational question since the physical ingredients of Einstein's theory have never been precisely specified on all scales. There are many unsolved problems relating to the coarse-graining, fitting, and averaging of geometry. In these lectures I will discuss these issues, with an emphasis on the timescape cosmology, which does at least provide a phenomenologically viable alternative to the standard model. In the timescape scenario, I have attempted to address the key issue of gravitational energy which I believe is intimately related to solving the riddle of "dark energy". It is my hope that if we pay close attention to observations, and think more deeply about fundamental concepts in light of new observations, that we might develop better statistical notions of gravitational energy and entropy, which may be important not only for cosmology at large but also for the foundations of gravitational physics.

2. THE FITTING PROBLEM: WHAT IS DUST?

2.1. On what scale are Einstein's equations valid?

In the standard FLRW cosmology, fundamental observers are defined to be "comoving with the dust" in geometries that are solutions to Einstein equations with a dust or perfect fluid source. This poses two problems. Firstly, it involves an extrapolation of Einstein's field equations

$$G^{\mu}{}_{\nu} = \frac{8\pi G}{c^4} T^{\mu}{}_{\nu} \qquad (1)$$

far beyond the scales on which they have been tested. General relativity is only well tested for isolated systems – such as the solar system or binary pulsars – for which $T^{\mu}{}_{\nu} = 0$.

Secondly, the notion of what a "dust particle" is in cosmology is not rigorously defined. The scale over which matter fields are coarse-grained to produce the energy–momentum tensor on the r.h.s. of (1) is not prescribed, leaving an inherent ambiguity. Traditionally, galaxies have been thought of as particles of dust. However, our observations show that galaxies themselves are not homogeneously distributed. The largest typical nonlinear structures are voids of diameter $30\,h^{-1}$Mpc [2]–[4], so that we must coarse grain on scales at least a few times larger to obtain a notion of statistical homogeneity. This process of coarse-graining involves unexplored statistical aspects of general relativity, which have barely been studied.

There is no ambiguity in applying Einstein's equations (1) to a fluid of particles with well-defined properties, such as ions, atoms and molecules in the early phases of the universe's expansion. However, as soon as gravitational collapse occurs then particle geodesics cross. Phase transitions occur, so the definition of the particles in the fluid approximation must change, giving rise to the following hierarchy of coarse-grained 'particles' in the epochs following last scattering:

1. Atomic, molecular, ionic or nuclear particles: applicable with
   - dust equation of state within any expanding regions which have not yet undergone gravitational collapse;
   - fluid equation of state within relevant collapsed objects (stars, white dwarfs, neutron stars) for periods of time between phase transitions that alter the non-gravitational particle interactions and the equation of state;
2. Collapsed objects such as stars and black holes coarse-grained as isolated objects;
3. Stellar systems coarse-grained as dust particles within galaxies;
4. Galaxies coarse-grained as dust particles within clusters;
5. Clusters of galaxies coarse-grained as bound systems within expanding filaments and walls;
6. Voids, walls and filaments combined as expanding regions of different densities in a single smoothed out cosmological fluid.

2.2. Coarse–graining

Any coarse-graining procedure amounts to replacing the microphysics of a given spacetime region by some collective degrees of freedom of those regions which are sufficient to describe physics on scales larger than the coarse-graining scale. Einstein's equations were originally formulated with the intent that the energy-momentum tensor on the r.h.s. of (1) should either describe fundamental fields, such as the Maxwell field, or alternatively to the coarse-graining of the purely nongravitational interactions described by such fields in the fluid approximation.

Up to step 3 in the hierarchy, there are no real problems of principle with coarse-graining since we are coarse-graining only over matter degrees of freedom which appear exclusively in the energy-momentum tensor. In 1917 when Einstein first applied general relativity to cosmology [8], this was sufficient since it had yet to be established that nebulae were distant galaxies, and the prevailing view was that the density of the universe was the density of the Milky Way. Decades later Einstein did consider the fitting problem, when he built the Swiss cheese model in collaboration with Straus [9]. However, this is a simple model which treats inhomogeneities as Schwarzschild solutions placed in holes in a homogeneous isotropic FLRW background. It deals with an idealized situation which is far simpler than the actual cosmic web, which astronomers really only began to uncover in the 1980s.

The fundamental problem then, is that since the universe is composed of a hierarchy of long-lived structures much larger than those of stars, we must also coarse-grain over the gravitational interactions within that hierarchy to arrive at a fluid description for

cosmology. With such a coarse-graining, geometry no longer enters purely on the left hand side of Einstein's equations but in a coarse-grained sense can be hidden inside effective fluid elements of a smoothed out energy-momentum tensor on the right hand side of (1). We have a complex hierarchical fitting problem [10, 11] that must be solved to relate the average geometry of the universe to the local geometry to which our clocks and rulers are calibrated.

The fundamental quantities of interest as the sources of the right hand side of Einstein's equations are those of mass–energy, momentum and angular momentum. Effectively, if we demand that equations (1) should also apply in a coarse-grained version on cosmological scales, then it means that we are seeking collective mass–energy parameters which average over the rotational kinetic energies of galaxies, binding energies of galaxies and clusters, kinetic energies of galaxies in virialized clusters, regional spatial curvature etc. Furthermore we must approach the problem more than just once, on a succession of scales. This necessarily involves the issue of quasilocal gravitational energy, and more particularly statistical properties of the gravitational interactions of bound systems.

Since we are no longer dealing with a fixed spatial metric this problem is far more complicated than any equivalent problem in Newtonian theory, and indeed it is largely unexplored territory. The physical degrees of freedom which we must coarse grain are contained in the curvature tensor and the sources of the field equations (1). In principle coarse-graining the curvature tensor might involve steps other than simply coarse-graining of the metric. However, if a metric description of gravity is assumed at each level, then schematically the hierarchy of coarse-graining might be heuristically described as

$$\left.\begin{array}{r} g_{\mu\nu}^{\text{stellar}} \rightarrow g_{\mu\nu}^{\text{galaxy}} \rightarrow g_{\mu\nu}^{\text{cluster}} \rightarrow g_{\mu\nu}^{\text{wall}} \\ \vdots \\ g_{\mu\nu}^{\text{void}} \end{array}\right\} \rightarrow g_{\mu\nu}^{\text{universe}} \tag{2}$$

where the ellipsis denotes the fact that the metric of more than one type of wall or void might possibly be relevant. In this scheme the lowest members are assumed to be well modeled by exact solutions of Einstein's field equations: $g_{\mu\nu}^{\text{stellar}}$ being a solution to the vacuum field equations with a star or black hole source (given by the Schwarzschild or Kerr solution), and $g_{\mu\nu}^{\text{void}}$ being that of a region filled with low density ionic dust with whatever symmetries are relevant.

Within the hierarchy (2) there are (at least) three steps that involve the coarse-graining of gravitational degrees of freedom, which might be summarized as

- *Galactic dynamics*: $g_{\mu\nu}^{\text{stellar}} \rightarrow g_{\mu\nu}^{\text{galaxy}}$;
- *Cluster dynamics*: $g_{\mu\nu}^{\text{galaxy}} \rightarrow g_{\mu\nu}^{\text{cluster}}$;
- *Cosmological dynamics*: $g_{\mu\nu}^{\text{cluster}} \rightarrow \left\{ g_{\mu\nu}^{\text{wall}} \oplus \cdots \oplus g_{\mu\nu}^{\text{void}} \right\} \rightarrow g_{\mu\nu}^{\text{universe}}$.

The gravitational degrees of freedom that are coarse-grained in galactic and cluster dynamics involve the gravitational binding energies of bound systems of different scales. By contrast cosmological dynamics deals with the coarse-graining of expanding regions of different densities, i.e., with the coarse-graining of the kinetic energy of expansion of space.

In the Newtonian cosmology [12] for particles of mass m with positions $r^i = a(t)x^i$, ($x^i =$const), relative to an arbitrary centre, the Friedmann equation

$$\frac{\dot{a}^2}{a^2} + \frac{kc^2}{a^2} = \frac{8\pi G\rho}{3} \tag{3}$$

is obtained from the Newtonian energy equation, $T - U = -V$, where $T = \frac{1}{2}m\dot{a}^2x^2$ is the kinetic energy per particle, $V = -\frac{4}{3}\pi G\rho a^2x^2m$ is the potential energy per particle and $U = -\frac{1}{2}kmc^2x^2$ is the total energy per particle, where k is a constant. Eq. (3), the Hamiltonian constraint of the full Einstein equations for the standard cosmology, is thus recognized to contain terms related to gravitational potential and binding energy, V, and the kinetic energy of expansion, T, in the Newtonian limit.

As long as the universe is perfectly homogeneous then these quantities are the same for all observers. However, once there is inhomogeneity, and in particular once there are gradients in spatial curvature, then these concepts become entangled. On account of the strong equivalence principle, spatial curvature cannot be defined at a point, and any definition necessarily involves a regional *quasilocal* definition. Gravitational binding energy and the kinetic energy of expansion are thus quasilocal concepts tied to gradients in spatial curvature.

2.3. Coarse–graining of bound systems

A statistical description of cosmological relativity involves both gravitational binding energy and the kinetic energy of expansion. It happens that the coarse-graining of these respective gravitational degrees of freedom relates to the scales at which the phenomena of dark matter and dark energy are respectively observed. It is therefore possible that both phenomena are related to different aspects of the same problem, namely that the standard model incorporates a rigidity of spatial curvature which is not demanded by full general relativity.

Since the coarse-graining of gravitational binding energy and the kinetic energy of expansion involve different physical questions, it may be prudent to investigate just one problem at a time. The timescape scenario [13]–[16] has been developed to deal with the problem of the kinetic energy of expansion only: in the approach taken thus far all coarse-grained regions are expanding ones. We will see in Sec. 5 that agreement with observation is obtained only by incorporating a fraction of nonbaryonic dark matter. However, we must remain open-minded as to whether the parameter found corresponds to actual new particles as in the standard Λ Cold Dark Matter (ΛCDM) model, or whether is a simply a phenomenological parameter that accounts for the coarse-graining of binding energy that we have not yet examined.

A piece of evidence in support of an alternative to conventional CDM is the remarkable phenomenological success of Modified Newtonian Dynamics (MOND) [17, 18] at the level of galactic dynamics. This empirical model works well at galactic levels, but fails at the cluster level. While galactic and cluster dynamics both involve binding energy, the kinetic energy degrees of freedom of the two situations are different. Galactic dynamics typically involves stars in rotationally supported structures, whereas cluster

dynamics involves the less coherent motions of galaxies which move in the combined potential but also interact with each other in random pairwise encounters. Whereas the diameters of stars are very small ($< 10^{-5}\,\%$) compared to their interparticle separations in galaxies, the typical size of a galaxy is a more sizable fraction (0.5–$15\,\%$) of typical intergalactic distances in a virialized cluster.

Newtonian dynamics is used almost exclusively in the treatment of both galaxy and cluster dynamics. The rationale for this is that fields are weak. However, even if spacetime is close to a Minkowski background, an important question remains: *which* Minkowski background? There is no global Minkowski background in the universe, and even if space is close to Minkowski for small time intervals on a spatial 2-sphere encompassing a galaxy or galaxy cluster, then the question remains: how do we calibrate the rulers and clocks on that 2-sphere relative to another similar 2-sphere elsewhere? Gravitational lensing calculations make use of a formula derived for the ideal Schwarzschild geometry of an isolated point mass, which has an exact timelike Killing vector. Are there pitfalls in applying such notions of mass to circumstances in which there are no pure timelike Killing vectors, and no truly isolated masses? To my knowledge, these questions have not been rigorously posed in general relativity, let alone answered.

Some attempts have been made to understand galaxy rotation curves with exact dust solutions [19]–[21]. However, the applicability of these solutions as alternatives to galactic dark matter has been debated [20, 22]. Furthermore, while new exact solutions to Einstein's equations may offer new insights into the possibilities offered by general relativity, they do not directly address the problems posed by coarse-graining. They are also limited by the additional restrictions that must be applied to reduce Einstein's equations to a soluble form. For example, although galaxy clusters are often spherical in shape the spherically symmetric dust Lemaître–Tolman–Bondi (LTB) solutions [23]–[25] cannot be applied[2] to virialized clusters, since galaxies in clusters do not collapse inwards in coherent spherical shells. Even if the motion of individual galaxies is close to radial, the phases of the galaxies relative to passage through the centre of the cluster are completely uncorrelated. Individual galaxies will pass close to the core of the cluster and emerge from the other side; but at any instant the number of galaxies moving out from the centre might be comparable to the number falling in.

In my view the problems of coarse-graining of galaxies and clusters are difficult. However, in view of the phenomenological successes of MOND at the galactic scale [17, 18] we should be open to the possibility that simplifying principles remain to be discovered.

2.4. Coarse–graining the cosmological fluid

The final step of coarse-graining involves qualitatively new fundamental questions. If we require a single model to describe the evolution of the universe from last scattering to the present day, then we must coarse grain on scales over which the notion of a

[2] By contrast LTB models are clearly applicable to individual expanding spherical voids [26] with ionic or molecular sized dust.

dust ‘particle’ has a meaning from last scattering up to the present. The description of a galaxy composed of stars, or of a virialized galaxy cluster composed of galaxies is only valid for those epochs after which the relevant ‘particles’ have formed and are themselves relatively unchanging. Over cosmological timescales we do not have well-defined invariant dust particles. The nature of galaxies and galaxy clusters changes through growth by accretion of gas and by mergers.

To get around the problem of ill-defined particle-like building blocks, an appropriate strategy is to coarse-grain the ‘dust’ on scales large enough that the *average* flow of mass from one cell to another is negligible up to the present epoch. Although galaxy clusters vary greatly in size and complexity, there are no common virialized structures larger than clusters. Thus coarse-graining on scales larger than clusters necessarily means dealing with fundamental objects that are themselves *expanding*, i.e., with entities that resemble *fluid elements* in hydrodynamics rather than point particles.

Another qualitative difference from the case of bound systems is that we have to deal with expanding fluid elements that have vastly different densities at the present epoch, and which evolve more or less independently. Although we can receive signals from anywhere within our particle horizon, the energy we receive in electromagnetic and gravitational waves, or indeed in cosmic ray particles from distant galaxies, is negligible in comparison with the rest-energy of the local density field. The region which has contributed matter particles to define the local geometry of our own galaxy is actually very small. This bounding sphere, which Ellis and Stoeger [27] call the *matter horizon*, is estimated by them to be of order $2\,$Mpc for the Milky Way using assumptions about the growth of perturbations from the standard cosmology. This scale also coincides roughly with the scale at which the Hubble flow is believed to begin in the immediate neighbourhood of the Local Group of galaxies. It is one way of realizing the concept of *finite infinity*, introduced qualitatively by Ellis in his first discussion of the fitting problem [10].

For galaxy clusters some sort of finite infinity notion – which we will better define in Sec. 5 – with a variable scale of order 2–$10\,$Mpc depending on the size of cluster might be useful for defining the minimum smoothing scale containing bound structures. By combining such regions we arrive at the walls and filaments that contain most of the mass of the universe. However, to this we must also add the voids which dominate the volume of the universe at the present epoch. These are the regions in which structures have never formed, and which still contain the same ionic, atomic and molecular dust content that has existed since very early epochs, only greatly diluted by expansion.

If we set aside a few peculiar large wall structures [28], then the largest *typical* nonlinear structures are voids. Surveys indicate that voids with characteristic mean effective radii[3] of order $(15 \pm 3)\,h^{-1}$Mpc (or diameters of order $30\,h^{-1}$Mpc), and a typical density contrast of $\delta\rho/\rho = -0.94 \pm 0.02$, make up 40% of the volume of the nearby universe [2, 3]. A recent study [4] of the Sloan Digital Sky Survey Data Release 7 finds a median effective void radius of $17\,h^{-1}$Mpc, with voids of effective radii in

[3] Voids display a degree of ellipticity. The *mean effective radius* of a void is that of a sphere with the same volume as occupied by the void [2]–[4], which is typically larger than the maximal sphere enclosed by the same void.

the range $10\,h^{-1}$Mpc to $30\,h^{-1}$Mpc occupying 62% of the survey volume. In addition to these there are numerous smaller minivoids [5], which combined with the dominant voids ensure that voids dominate the present epoch universe by volume.

2.4.1. Coarse-graining at the statistical homogeneity scale

Any minimal scale for the cosmological coarse-graining of the final smoothed density distribution has to be substantially larger than the diameter of the largest typical structures. Void statistics [4] indicate an effective cutoff of $60\,h^{-1}$Mpc for the largest mean effective diameters of voids, i.e., twice the scale of the typical dominant void diameters. Thus observationally, the relevant scale for coarse-graining appears to be of order two to three times the dominant void diameter, e.g., of order $100\,h^{-1}$Mpc. Although the scale of transition to statistical homogeneity is debated [29, 30] recent results from the WiggleZ survey suggest that the transition occurs in the range[4] $70\,h^{-1}$–$100\,h^{-1}$Mpc [31].

A statistical homogeneity scale of $\sim 100\,h^{-1}$Mpc also coincides roughly with the Baryon Acoustic Oscillation (BAO) scale [32, 33], $D_{\rm BAO}$. Physically there is a good reason for this coincidence. The BAO scale is that of the largest acoustic wave in the plasma at last scattering. For scales larger than this the spectrum of initial density perturbations is roughly scale invariant with a density contrast $\delta\rho_B/\rho_B \sim 10^{-5}$ in baryons, and $\delta\rho_C/\rho_C \sim 10^{-4}$ in cold dark matter. Below the BAO scale initial density contrasts may be amplified by acoustic waves in the plasma, so the amplitude of initial density contrasts is somewhat larger, particularly at the scales associated with the higher order odd acoustic peaks. The BAO scale therefore provides a demarcation between the linear and nonlinear regimes of the subsequent growth of structure.

At first, it might seem contradictory that the amplification of the primordial density perturbations corresponding to the first acoustic peak should give a small enhancement which in the standard ΛCDM model can treated in the linear regime of perturbation theory with good observational agreement, whereas higher order peaks give enhancements which give rise to a nonlinear regime. However, it must also be remembered that perturbations are nested, so that in some cases we get amplifications on top of amplifications. Characteristic features will arise from the fact that at last scattering the odd acoustic peaks corresponds to compression in gravitational potential wells and rarefaction in potential peaks, whereas the even acoustic peaks correspond to rarefaction in potential wells and compression in potential peaks. The odd peaks will thus produce increasing amplifications of structure, while even peaks will somewhat undo the amplifications (but not completely on account of baryon drag).

The fact that the diameter of the dominant voids at $D_{\rm void} \sim 30\,h^{-1}$Mpc [2]–[4] is close to one third of $D_{\rm BAO}$ is seen to be a consequence of these structures growing from the additional amplification provided by the third acoustic peak[5]. Since voids are regions

---

[4] This range represents the range of bias-corrected values listed for various redshift ranges in Table 4 of ref. [31]. These estimates assume a ΛCDM model and use data in the redshift range $0.1 < z < 0.9$.

[5] This corrects statements made in Sec. V of ref. [15], where on account of a confusion about the role of the odd and even acoustic peaks it was incorrectly suggested the second peak should provide a relevant

which appear to expand at faster rates[6] than walls, with density contrasts growing to $\delta\rho/\rho \to -1$ at late times, the exact ratios of scales of the acoustic peaks at last scattering are not preserved in the nonlinear regime today. In fact, a precise measurement of the difference between the ratio $D_{\rm void}/D_{\rm BAO}$ and $1/3$ would provide useful constraints on the variation of the Hubble parameter in the nonlinear regime. Since voids are the dominant nonlinear structures in the cosmic web, the beginning of an emergence of a notion of homogeneity at scales $\sim 70\,h^{-1}$Mpc [31] may be related cutoff in the statistics of void diameters at $60\,h^{-1}$Mpc found by Pan *et al.* [4], rather than a scale related to the second acoustic peak. Since the even acoustic peaks represent deamplified initial density contrasts, they are unlikely to have very clear-cut signatures in cosmic structure.

2.4.2. Variations on scales larger than the statistical homogeneity scale

In the standard cosmology it is often assumed that as the domain $\mathcal{D}$ of a spatial average is made larger and larger at the present epoch, the density contrast $\langle\delta\rho/\rho\rangle_{\mathcal{D}}$ will diminish to small values which match those at the last scattering epoch. However, this assumes constraints on the notion of statistical homogeneity over and above[7] those required for a universe that has evolved from an initial density perturbation spectrum that was close to scale-invariant, as is consistent with the observed CMB anisotropies and primordial inflation. Given initial nested density fluctuations on arbitrarily large spatial scales, then if any arbitrarily large domain $\mathcal{D}$ evolves independently by close to FLRW evolution, its density at the present epoch will always have evolved from a perturbation that was within the initial spectrum, but not necessarily exactly the mean.

We can therefore crudely estimate the standard deviation of the density of cells on scales larger than $100\,h^{-1}$Mpc by assuming that each cell evolves as an independent Friedman universe from a smooth perturbation at the epoch of last scattering. (This assumes that the backreaction contributions to be discussed in Sec. 3 do not dominate the volume–average evolution.) Using the Friedmann equation with pressureless dust only, for which

$$a_0^2 H_0^2 (\Omega_{M0} - 1) = a^2(t) H^2(t) [\Omega_M(t) - 1],$$

we obtain a present epoch density contrast

$$\delta\rho_0 \simeq \left(\frac{H}{H_0}\right)^2 \frac{\delta\rho_t}{(1+z)^2}\,. \tag{4}$$

---

scale to voids and the third peak to clusters of galaxies. The scale of rich clusters of galaxies is more likely to result from the nonlinear evolution of the fifth peak amplification.

[6] Here we refer to the rate as measured by any one observer. Calibrating the expansion rate with different canonical clocks is an essential ingredient of the timescape cosmology which we will return to in Sec. 5

[7] In particular, perturbations on different scales would need to compensate each other in such a way as to maintain a homogeneous isotropic universe which is at present within 1% of being spatially flat overall. In the standard model with FLRW evolution this is required to fit the overall angular scale of the acoustic peaks in the CMB. We will see in Sec. 6.2 that in the timescape model the acoustic scale can be fit without such a restriction on spatial curvature.

Here the density contrast is relative to the critical density, so that $\delta\rho_t = \Omega_{_M}(t) - 1$ etc, where $\Omega_{_M}$ is a density parameter for the isolated region only. Thus if we take $\delta\rho_t \simeq 10^{-4}$ at last scattering (for a CDM density contrast), when $z \simeq 1090$ and when evolution is roughly matter-dominated with $H \simeq 2/(3t)$ and $t \simeq 380,000\,\mathrm{yr}$, we are led to $\delta\rho_{_0} \simeq 0.025/h^2 \simeq 0.06$ if $h \simeq 0.65$.

This crude estimate can be compared to the actual density variance determined from large scale structure surveys [29, 30]. Sylos Labini *et al*. [30] determined the variance in the number density of luminous red galaxies (LRGs) in the SDSS-DR7 by dividing the full sample of 53,066 galaxies in the redshift range $10^{-4} < z < 0.3$ into N equal nonoverlapping volumes. Over the range $4 \leq N \leq 15$, they found a standard deviation of order 8%, consistent with an earlier measurement of 7% by Hogg *et al*. [29] in a smaller LRG sample. These values are very close to our order of magnitude estimate of 6%, which has still not been corrected to include radiation at last-scattering, or the effects of backreaction at late epochs.

Given a nearly scale–invariant spectrum of nested density perturbations, we expect that the variance in density should not decrease appreciably if sample volumes are increased at nearby redshifts. In principle, it should be possible to calculate the variance as a function of scale, given the constraints from the CMB anisotropy spectrum at long wavelengths. For spatial slices at higher redshifts, looking further back in time, the variance would decrease in accord with (4) – provided that a sample of objects such as LRGs can be found which does not exhibit strong evolutionary effects over the range of redshifts in question.

In summary, in order to coarse-grain fluid cells in such a way that the size of a cell is larger than the largest typical nonlinear structures, with a mass that does not change on average from last scattering until today, observations show that we should coarse-grain fluid cells at a scale of order $70\,h^{-1}$–$100\,h^{-1}$Mpc. This scale will be called the statistical homogeneity scale (SHS). Such a scale marks the transition from a nonlinear regime in which there is a very large variance in $\delta\rho/\rho$, to a regime in which cosmological average evolution with a single Hubble parameter becomes well defined. It does not mark a scale at which average evolution necessarily becomes precisely FLRW, nor at which density contrasts become completely negligible. Rather variations on spatial scales larger than the SHS at the present epoch are bounded by a maximum $\delta\rho/\rho \lesssim 0.1$, as is consistent with observations.

In this subsection we have presented a summary of observational results to be accounted for in cosmological coarse-graining, without assuming any details about backreaction. There is one other observational puzzle which also requires mention: the Sandage-de Vaucouleurs paradox[8]. This is the puzzle that in conventional ways of thinking, we should expect large statistical scatter in the peculiar velocities of galaxies below the SHS, if they are indeed "particles of dust". In fact, on scales of order $20\,$Mpc the statistical scatter should be so large that no linear Hubble law can be extracted. Yet

[8] In the literature this has been called the "Hubble–de Vaucouleurs paradox" [34, 35] and alternatively the "Hubble–Sandage paradox" [36]. However, the paradox never involved Hubble directly, but was originally raised by Sandage and collaborators [37] in objection to de Vaucouleurs' hierarchical cosmology [38] before strong evidence for the cosmic web of voids, sheets and filaments had amassed.

$20\,$Mpc is the very scale on which Hubble originally found his famous linear law. This statistical quietness of the local Hubble flow is difficult to reconcile with conventional understanding. In any FLRW universe which expands forever, peculiar velocities do decay. However, the ΛCDM parameters required for the velocity dispersion predicted by structure formation to match the observed velocity dispersion, do not coincide with the concordance parameters [39].

2.5. Approaches to coarse-graining

The problem of coarse-graining in general relativity in a bottom-up fashion is little studied. In principle, it is a very interesting question, which should deal, e.g., at the galactic level with the problem of replacing the Weyl curvature of individual Schwarzschild or Kerr solutions by a coarse-grained Ricci curvature for a dust fluid. Higher levels of coarse-graining in the hierarchy (2) involve further physical questions. Rather than dealing with multi-scale problems, the few existing studies simplify the hierarchy (2) to a single step.

2.5.1. Covariant coarse-graining

Korzyński [40] has proposed a covariant coarse-graining procedure, which could conceivably be applied to any step in the hierarchy (2) for which the starting point is the metric of a known dust solution. Korzyński's idea is to isometrically embed the boundary of a comoving dust-filled domain – required to have S^2 topology with positive scalar curvature – into a three-dimensional Euclidean space, and to construct a "fictitious" three-dimensional fluid velocity which induces the same infinitesimal metric deformation on the embedded surface as the "true" dust flow does on the domain boundary in the original spacetime. This velocity field is used to uniquely assign coarse-grained expressions for the volume expansion and shear to the original domain. An additional construction using the pushforward of the Arnowitt-Deser-Misner (ADM) shift vector [41] is used to similarly obtain a coarse-grained vorticity. The coarse-grained quantities are quasilocal functionals which depend only on the geometry of the boundary of the relevant domain. This formalism is at an early stage of development, but could conceivably provide new methods for attacking the fitting problem.

2.5.2. Discretized universes

The Lindquist–Wheeler model [42] is a lattice based approach, which has received new interest recently [43]–[46]. The coarse-graining hierarchy (2) is replaced by the simplified scheme

$$g_{\mu\nu}^{\text{Schwarzschild}} \to g_{\mu\nu}^{\text{universe}} \tag{5}$$

with the proviso that $g_{\mu\nu}^{\text{universe}}$ does not represent a continuum metric in the usual sense. Rather, by matching the spherical boundaries of radially expanding geodesics in the

Schwarzschild geometries of a regular lattice of equal point masses, the Friedmann equations are obtained [42, 43]. The matching is exact only at the points where the radial spheres intersect and is approximate in the regions in which spheres overlap or are excluded. A continuum cosmological geometry is thus realized only approximately.

This model is analogous to the Swiss cheese models [9] in the sense that the point group symmetry of the lattice is a discretized version of a system with overall global spatial homogeneity. Ray-tracing studies in the spatially flat Lindquist–Wheeler model lead to results which are almost identical to that of the exact Einstein-de Sitter solution[9]. While this demonstrates that the Lindquist–Wheeler does provide a consistent lattice description of the FLRW models, it unfortunately does not give any indication of how one should treat the problem of inhomogeneity, without discrete symmetries.

3. AVERAGING AND BACKREACTION

The terms "coarse-graining" and "averaging" are often used interchangeably in a loose sense. However, whereas coarse-graining is generically a bottom-up process, averaging is top-down: one is interested in the overall average dynamics and evolution, usually without direct consideration of the details of the course-graining procedure. Whereas coarse-graining is little studied, considerably more attention has been paid to averaging. Several approaches have been pursued and are discussed in many reviews including, e.g., those of Buchert [48, 49], van den Hoogen [50] and Clarkson *et al*. [51].

Cosmological averaging typically starts from the assumption that a well-defined average exists, with a number of assumed properties. If one assumes that the Einstein field equations (1) are valid for some general inhomogeneous geometry, $g_{\mu\nu}$, then given some as yet unspecified averaging procedure denoted by angle brackets, the average of (1) gives

$$\langle G^{\mu}{}_{\nu}\rangle = \langle g^{\mu\lambda}R_{\lambda\nu}\rangle - \tfrac{1}{2}\delta^{\mu}{}_{\nu}\langle g^{\lambda\rho}R_{\lambda\rho}\rangle = \frac{8\pi G}{c^4}\langle T^{\mu}{}_{\nu}\rangle\,. \tag{6}$$

A number of choices are possible at this point since there is no *a priori* reason to assume that $\langle G^{\mu}{}_{\nu}\rangle$ is the Einstein tensor of an exact geometry.

In the *macroscopic gravity* approach, Zalaletdinov [52]–[54] takes the average inverse metric $\langle g^{\mu\nu}\rangle$ and the average Ricci tensor $\langle R_{\mu\nu}\rangle$ as basic variables, so that

$$\langle g^{\mu\lambda}\rangle\langle R_{\lambda\nu}\rangle - \tfrac{1}{2}\delta^{\mu}{}_{\nu}\langle g^{\lambda\rho}\rangle\langle R_{\lambda\rho}\rangle + C^{\mu}{}_{\nu} = \frac{8\pi G}{c^4}\langle T^{\mu}{}_{\nu}\rangle\,, \tag{7}$$

where the correlation functions $C^{\mu}{}_{\nu}$ are defined by the difference of the left hand sides of (7) and (6). Zalaletdinov provides additional mathematical structure to prescribe a covariant averaging scheme, thereby defining properties of the correlation functions.

Alternatively one can consider the difference of the general inhomogeneous metric and the averaged metric

$$g_{\mu\nu} = \bar{g}_{\mu\nu} + \delta g_{\mu\nu}, \tag{8}$$

[9] A different result was first claimed in an earlier study [43], but then corrected [46]. The review article [47] was written before the corrected result [46] was found, and it cites the earlier incorrect result.

where $\bar{g}_{\mu\nu} \equiv \langle g_{\mu\nu} \rangle$, with inverse $\bar{g}^{\lambda\mu} \neq \langle g^{\lambda\mu} \rangle$. One may now determine a connection $\bar{\Gamma}^{\lambda}{}_{\mu\nu}$, curvature tensor $\bar{R}^{\mu}{}_{\nu\lambda\rho}$ and Einstein tensor $\bar{G}^{\mu}{}_{\nu}$ based on the averaged metric, $\bar{g}_{\mu\nu}$, alone. The differences $\delta\Gamma^{\lambda}{}_{\mu\nu} \equiv \langle \Gamma^{\lambda}{}_{\mu\nu} \rangle - \bar{\Gamma}^{\lambda}{}_{\mu\nu}$, $\delta R^{\mu}{}_{\nu\lambda\rho} \equiv \langle R^{\mu}{}_{\nu\lambda\rho} \rangle - \bar{R}^{\mu}{}_{\nu\lambda\rho}$, $\delta R_{\mu\nu} \equiv \langle R_{\mu\nu} \rangle - \bar{R}_{\mu\nu}$ etc, then represent the *backreaction* of the averaged inhomogeneities on the average geometry determined from $\bar{g}_{\mu\nu}$. Furthermore, the average Einstein field equations (6) may be written

$$\bar{G}^{\mu}{}_{\nu} + \delta G^{\mu}{}_{\nu} = \frac{8\pi G}{c^4} \langle T^{\mu}{}_{\nu} \rangle \,. \tag{9}$$

This expresses the fact that the Einstein tensor of the average metric is not in general the average of the Einstein tensor of the original metric. The processes of averaging and constructing the Einstein tensor do not commute.

Equation (6) and (9) are of course very similar, but may differ in both the definition of the average represented by the angle brackets, and also in the split of the background averaged Einstein tensor and the correlation or backreaction terms. The manner in which averaging schemes differ often relate to whether the effects of backreaction are assumed to be weak or strong.

3.1. Weak backreaction: the Friedmann–Lemaître universe as the average

The remarkable success of the standard cosmology, albeit with sources of dark matter and dark energy which have not been directly observed, has understandably led most researchers to assume that it must be correct, even if only in an average sense. As a consequence, many researchers simply begin from the starting point that the FLRW geometry must be the average, or very close to the average evolution.

One can then either assume that

- there is no backreaction on average evolution but inhomogeneities are sufficiently large that they significantly affect the propagation of light, as in the Swiss cheese [55, 56] and meatball [57] models; or
- backreaction is sufficiently small that the changes to average evolution can be treated perturbatively about a homogeneous isotropic background, at least initially.

The second approach, *weak backreaction*, is of course intimately related to standard cosmological perturbation theory. One assumes that the average geometry $\bar{g}_{\mu\nu}$ of (8) is exactly FLRW, and that the quantities $\delta g_{\mu\nu}$ can be treated as perturbative corrections.

The issue of whether backreaction is significant or insignificant in the perturbative FLRW context is a matter of much debate, with different authors coming to different conclusions, which may be traced to various differences in assumptions made. These issues are discussed in many reviews, such as those of Clarkson *et al*. [51] and Kolb [58], and will not be discussed in detail here. In my view this debate shows that there are potential problems, which cannot be resolved by staying within perturbation theory.

In fact, all researchers are well aware that there is a nonlinear regime in structure formation, which is explored by N-body simulations in the standard cosmology. Since there is as yet no rigorous procedure for coarse-graining the gravitational degrees of

freedom which describe the small-scale structures, the perturbative approach can only be valid given an implicit assumption that there is no new physics to be found when coarse-graining the hierarchy (2).

Such an assumption underlies a typical argument against backreaction: if we *assume* a FLRW geometry, and estimate the magnitude of the perturbations using typical rotational and peculiar velocities of galaxies, then the corrections are small [59]. However, at late epochs galaxies and galaxy clusters are not homogeneously distributed, and cannot be considered as randomly distributed gas particles on scales of tens of megaparsecs below the SHS. The dominant structures on these scales are voids of diameter $\sim 30\,h^{-1}$Mpc with density contrasts $\delta\rho/\rho \sim -0.95$ [2, 3]. Using galaxy peculiar velocities as an estimate of $\delta\rho/\rho$ is therefore misplaced. There is no direct evidence that a spatially homogeneous geometry is the correct one below the SHS.

It may thus simply be incorrect to assume that a FLRW model exactly describes the average evolution of the universe at the largest scales for all times. Approaches which do not make the restrictive assumption of average FLRW evolution are those with *strong backreaction*.

3.2. Strong backreaction: Spacetime and spatial averages

If Einstein's equations for a single metric with a prescribed energy-momentum tensor source are not the relevant equations for describing the average evolution of the universe on cosmological scales, then new physical ingredients are required, either explicitly in the averaging formalism itself, or else implicitly in relating the results of a particular formalism to observations. After all, our measurements involve physical rulers and clocks adapted to a local geometry, and this local geometry must somehow be matched to the statistical geometry that describes average cosmic evolution.

Strong backreaction as a solution to the problem of dark energy elicits much confusion in the community, as typified by the statement that dark energy is *just* an issue of inhomogeneities, and that it is entirely solved *within* general relativity. Even advocates of strong backreaction might disagree with this statement, depending on what is meant by "general relativity". There is a widely held view, particularly among those not involved in general relativity research, that it consists solely of completed old physics. However, those better acquainted with general relativity know that even setting aside the regime of quantum gravity, general relativity is not a final complete theory, but contains many open and unsolved questions – in particular in relation to gravitational energy and entropy and the averaging problem.

Strong backreaction does involve new physics, but in my view the new physics must involve a natural extension of the principles of relativity into regimes which Einstein did not envisage when he wrote down his field equations in 1915. Whether one wishes to call it "general relativity" or "cosmological relativity" or something else is therefore a matter of taste. The essential point is that one is proposing new rules for the geometrical structure of spacetime on cosmological scales.

The cosmological spacetime is to be a statistical average geometry. Any process of taking an average will in general break the general covariance of Einstein's equations.

There are differing approaches to this, which alternatively involve spacetime or spatial averages. Many mathematical approaches exist, including Ricci flow [60]–[63], group averaging of the FLRW isometry group [64], covariant frame-bundle averaging [65] and constant mean (extrinsic) curvature (CMC) flows [66, 67]. Here I will just very briefly outline the two approaches which have attracted the most attention, largely due to Zalaletdinov and Buchert.

3.2.1. Zalaletdinov's macroscopic gravity

Zalaletdinov has developed a theory called *macroscopic gravity* based on spacetime averages [52, 53, 54, 68]. His aim is to consistently average the Cartan equations from first principles, in analogy to the averaging of the microscopic Maxwell–Lorentz equations in electromagnetism. However, whereas electrodynamics is linear in the fields on the fixed background of Minkowski spacetime, gravity demands an averaging of the nonlinear geometry of spacetime itself and is considerably more complicated.

Additional mathematical structures are required to average tensors in a covariant manner on a given manifold, $\mathcal{M}$. To this end Zalaletdinov introduces bilocal averaging operators [52]–[54], $\mathcal{A}^{\mu}{}_{\alpha}(x,x')$, with support at two points $x \in \mathcal{M}$ and $x' \in \mathcal{M}$, which allow one to construct a bitensor extension, $\mathbf{T}^{\mu}{}_{\nu}(x,x')$, of a tensor $T^{\mu}{}_{\nu}(x)$ according to

$$\mathbf{T}^{\mu}{}_{\nu}(x,x') = \mathcal{A}^{\mu}{}_{\alpha'}(x,x')T^{\alpha'}{}_{\beta'}(x')\mathcal{A}^{\beta'}{}_{\nu}(x',x)\,. \tag{10}$$

The bitensor extension is then integrated over a 4-dimensional spacetime region, $\Sigma \subset \mathcal{M}$, to obtain a regional average according to

$$\bar{T}^{\mu}_{\ \nu}(x) = \frac{1}{\mathcal{V}_{\Sigma}}\int_{\Sigma} \mathrm{d}^4x' \sqrt{-g(x')}\,\mathbf{T}^{\mu}{}_{\nu}(x,x'), \tag{11}$$

where $\mathcal{V}_{\Sigma} \equiv \int_{\Sigma}\mathrm{d}^4x\sqrt{-g(x)}$ is the spacetime volume of the region Σ. The bitensor transforms as a tensor at every point but is a scalar when integrated over a region for the purpose of averaging.

Macroscopic gravity is a general covariant averaging formalism, rather than an approach which was specifically formulated with cosmology in mind. In order to make contact with cosmology, additional assumptions have been made. For example, Paranjape and Singh considered a spatial averaging limit [69]. Other studies have made the assumption, similar to the weak backreaction approach, that the average geometry is FLRW [70]–[73]. In that case it was found that the macroscopic gravity correlation terms take the form of a spatial curvature, even though a spatially *flat* FLRW geometry was assumed for the average geometry [70].

In my view, although Zalaletdinov's formalism is mathematically elegant, it has weaknesses as a physical theory. In particular, it has been designed to closely resemble general relativity itself. Apart from the fact that it deals with two geometric scales – a microscopic one and a macroscopic one – there is no scale in the final theory. Cosmological observations suggest a particular hierarchy of scales (2), which may involve physical issues more complex than simply taking one step from a microscopic theory to a macroscopic theory of gravity. In particular, the coarse-graining of the gravitational degrees

of freedom involving binding energy at one level and the kinetic energy of expansion at another, may give rise to qualitatively new phenomena. Rather than seeking to mimic the steps involved in coarse-graining matter degrees of freedom, we need to specify macroscopic scales and physical principles relevant to coarse-graining in cosmology.

3.2.2. Buchert's spatial averaging formalism

In the late 1990s, building on earlier work [60, 74, 75], Buchert developed an approach [76, 77] for the spatial averaging of scalar quantities associated with the Einstein field equations (1), with cosmological averages in a fully nonperturbative setting in mind at the outset. He applied the $3+1$ ADM spacetime split [41], which is a natural approach if the Einstein field equations (1) are to be viewed as evolution equations.

Rather than tackling the mathematically difficult problem of averaging tensors, Buchert averaged scalar quantities in general inhomogeneous spacetimes with perfect fluid energy–momentum sources. Such scalars include the density, ρ, expansion, θ, and scalar shear, $\sigma^2=\frac{1}{2}\sigma_{\alpha\beta}\sigma^{\alpha\beta}$ etc. For an arbitrary manifold, one can always locally choose ADM coordinates,

$$\mathrm{d}s^2=-\boldsymbol{\omega}^0\otimes\boldsymbol{\omega}^0+g_{ij}(t,\mathbf{x})\,\boldsymbol{\omega}^i\otimes\boldsymbol{\omega}^j, \tag{12}$$

where $\boldsymbol{\omega}^0\equiv\mathcal{N}(t,\mathbf{x})\,c\,\mathrm{d}t$, and $\boldsymbol{\omega}^i\equiv\mathrm{d}x^i+\mathcal{N}^i(t,\mathbf{x})\,c\,\mathrm{d}t$ define the ADM lapse function, $\mathcal{N}$, and shift vector, $\mathcal{N}^i$. Such coordinates can only be chosen globally if one restricts the evolution problem to that of irrotational flow, as Buchert does. In that case (12) may be assumed to apply over global $t=$const spatial hypersurfaces. For a dust source[10] we can then choose synchronous coordinates with $\mathcal{N}=1$ and $\mathcal{N}^i=0$. With these choices, the Einstein equations may be averaged on a domain, $\mathcal{D}$, of the spatial hypersurfaces, Σ, to give

$$3\frac{\dot{\bar{a}}^2}{\bar{a}^2} = 8\pi G\langle\rho\rangle-\tfrac{1}{2}c^2\langle\mathcal{R}\rangle-\tfrac{1}{2}\mathcal{Q}, \tag{13}$$

$$3\frac{\ddot{\bar{a}}}{\bar{a}} = -4\pi G\langle\rho\rangle+\mathcal{Q}, \tag{14}$$

$$\partial_t\langle\rho\rangle+3\frac{\dot{\bar{a}}}{\bar{a}}\langle\rho\rangle=0, \tag{15}$$

where an overdot denotes a t–derivative, and

$$\mathcal{Q}\equiv\frac{2}{3}\left\langle\left(\theta-\langle\theta\rangle\right)^2\right\rangle-2\langle\sigma^2\rangle=\frac{2}{3}\left(\langle\theta^2\rangle-\langle\theta\rangle^2\right)-2\langle\sigma^2\rangle\,, \tag{16}$$

is the *kinematic backreaction*. In these equations angle brackets denote the spatial volume average of a quantity, so that $\langle\mathcal{R}\rangle\equiv\left(\int_{\mathcal{D}}\mathrm{d}^3x\sqrt{\det{}^3g}\,\mathcal{R}(t,\mathbf{x})\right)/\mathcal{V}(t)$ is the average

[10] Extensions to perfect fluid [77] and other matter sources [78] have also been considered, as well as to general hypersurfaces tilted with respect to the fluid flow [79]–[83].

spatial curvature, for example, with $\mathcal{V}(t) \equiv \int_{\mathcal{D}} \mathrm{d}^3x\sqrt{\det{}^3g}$ being the volume of the domain $\mathcal{D} \subset \Sigma$. Note that $\bar{a}$ is *not* the scale factor of any given geometry, but rather is defined in terms of the average volume according to

$$\bar{a}(t) \equiv \left[\mathcal{V}(t)/\mathcal{V}(t_0)\right]^{1/3} . \tag{17}$$

It follows that the Hubble parameter appearing in (13)–(15) is related to the volume-average expansion scalar, θ, by

$$\frac{\dot{\bar{a}}}{\bar{a}} = \tfrac{1}{3}\langle\theta\rangle. \tag{18}$$

The condition

$$\partial_t\left(\bar{a}^6\mathcal{Q}\right) + \bar{a}^4c^2\partial_t\left(\bar{a}^2\langle\mathcal{R}\rangle\right) = 0, \tag{19}$$

is required to ensure that (13) is the integral of (14). In Buchert's scheme the non-commutativity of averaging and time evolution is described by the exact relation [74, 75, 76, 84]

$$\partial_t\langle\Psi\rangle - \langle\partial_t\Psi\rangle = \langle\Psi\theta\rangle - \langle\theta\rangle\langle\Psi\rangle \tag{20}$$

for any scalar, Ψ.

Eq. (14) is suggestive since it implies that if the backreaction term is large enough – e.g., for a large variance in expansion with small shear – then the volume average acceleration, $\bar{a}^{-1}\ddot{\bar{a}} = \frac{1}{3}\frac{\mathrm{d}}{\mathrm{d}t}\langle\theta\rangle + \frac{1}{9}\langle\theta\rangle^2$, could be positive, even if the expansion of all regions is locally decelerating. Although the fraction of the volume occupied by the faster expanding regions is initially tiny, this fraction may nonetheless become significant at late epochs, skewing the average to give an illusion of acceleration during the transition epoch to void domination. Whether this is observationally viable, however, depends crucially on: (i) how large the variance in expansion rates can grow given realistic initial constraints on density perturbations; and (ii) the operational interpretation of the Buchert formalism. Since Buchert's formalism is a statistical one, additional assumptions are required to relate solutions of the Buchert equations to cosmological observations. The timescape cosmology, to be discussed in Secs. 4, 5, provides such a scheme.

3.3. Notions of average spatial homogeneity

The relationship between average homogeneity and observations is crucial for the interpretation any averaging scheme for inhomogeneous cosmology. The very near isotropy of the CMB demonstrates that when photons travel to us from the surface of last scattering, they traverse a geometry which to a very good approximation must be isotropic in some average sense. If we assume a statistical Copernican principle, then we must also expect some sort of average notion of spatial homogeneity. The hard question is how to relate the observed averaged isotropy of the geometry on our past light cone to an appropriate notion of average spatial homogeneity.

Most cosmologists' physical intuition is guided largely by the FLRW models, within which average homogeneity can be characterized in (at least) three distinct ways:

(i) The notion of average spatial homogeneity is described by a class of ideal comoving observers with synchronized clocks.

(ii) The notion of average spatial homogeneity is described by average surfaces of constant spatial curvature (orthogonal to the geodesics of the ideal comoving observers).

(iii) The expansion rate at which the ideal comoving observers separate within the hypersurfaces of average spatial homogeneity is uniform.

While these notions coincide for the FLRW geometries, it is not generally the case once spatial homogeneity is only approximate rather than exact, given that spatial curvature is characterized by more than a single scalar.

Already in perturbation theory about FLRW models, one can specialize to spacetime foliations which preserve one of the notions (i)–(iii) of average spatial homogeneity more fundamentally than the other two. Among the foliations discussed in the classic work of Bardeen [85] we can recognize those of each type above: the *comoving hypersurfaces* (and related synchronous gauge) take property (i) as more fundamental; the *minimal shear hypersurfaces*[11] (and related Newtonian gauge) are one type of foliation for which property (ii) is more fundamental; and finally the *uniform Hubble flow hypersurfaces* take property (iii) as more fundamental.

Bičák, Katz and Lynden-Bell [86] have further analysed foliations of perturbed FLRW models, with a view to enabling gauge choices in which the rotations and accelerations of local inertial frames can be determined directly from local energy–momentum perturbations $\delta T^{\mu}{}_{\nu}$. They consider uniform Hubble flow hypersurfaces; uniform intrinsic scalar curvature hypersurfaces; and minimal shear hypersurfaces. The *uniform intrinsic scalar curvature hypersurfaces* provide a foliation in addition to those considered by Bardeen, which also take property (ii) as more fundamental. Having chosen hypersurfaces Bičák, Katz and Lynden-Bell further fix the gauge by adopting a condition similar to the minimal shift distortion condition of Smarr and York [87]. For each choice of hypersurface it then follows that the coordinates of local inertial frames are more or less uniquely determined by the energy–momentum perturbations $\delta T^{\mu}{}_{\nu}$. In this sense these gauges might be seen as embodying Mach's principle. They are substantially more restrictive than the commonly used synchronous gauge or the generalized Lorenz–de Donder gauge [86].

In the nonlinear regime, below the SHS, not all of the conditions (i)–(iii) can apply, even if they apply in some average sense on scales larger than the SHS. The question is should any of these notions apply *below* the SHS? The timescape scenario begins from the premise that a notion of uniform Hubble flow can be applied below the SHS, in a way which takes Mach's principle into the nonlinear regime, as we discuss in Sec. 4.

This will involve a reinterpretation of the Buchert formalism [76, 77], which grew as a generalization of averaging in Newtonian cosmology [74, 75], and is based on an ADM approach on constant time hypersurfaces of observers "comoving with the dust". Since the split of space and time is unique in Newtonian theory, from the Newtonian

[11] For scalar perturbations this becomes a zero–shear condition, i.e., $\mathcal{K}_{ij} - \frac{1}{3} g_{ij} \mathcal{K} = 0$, where $\mathcal{K}_{ij}$ is the extrinsic curvature, g_{ij} the intrinsic metric, and $\mathcal{K} \equiv \mathcal{K}^{\ell}{}_{\ell}$. For general perturbations the hypersurfaces are defined by $\left(\mathcal{K}_{ij} - \frac{1}{3} g_{ij} \mathcal{K}\right)_{|ij} = 0$, where the bar denotes a covariant derivative with respect to the intrinsic 3–metric.

viewpoint this is the only natural choice one can make. However, this is not the case in general relativity.

If particles of dust were invariant from the time of last scattering until the present, then there would be no physical ambiguity about the notion of "comoving with the dust". In such a case, a choice of constant time hypersurfaces with a synchronous gauge is well motivated. However, as discussed in Sec. 2.2, in order to consistently deal with both the particles of ionic dust in voids, and also with 'particles' of dust larger than galaxies, we have to coarse-grain at the SHS over fluid elements which are themselves expanding. This demands coarse-graining over the gravitational degrees of freedom relating to spatial curvature, the kinetic energy of expansion, and gravitational binding energy.

We will adopt the viewpoint that the Buchert time coordinate is a collective degree of freedom of spacetime regions when coarse-grained at the SHS, and that if we form thin sandwiches from such regions in the time direction then they can be combined as effective hypersurfaces on which the Buchert formalism can be applied. However, new physics applies within the coarse-grained cells, as we will discuss next.

4. TIMESCAPE SCENARIO: CONCEPTUAL FOUNDATIONS

In considering the averaging problem, it is inevitable that at some level one must deal with Mach's principle, which may be stated [12, 86]: *"Local inertial frames (LIFs) are determined through the distributions of energy and momentum in the universe by some weighted average of the apparent motions"*. Mach's principle strongly guided Einstein in developing general relativity as a theory in which spacetime is a relational structure. As Einstein stated in his first work on cosmology: "In a consistent theory of relativity there can be no inertia relatively to 'space', but only an inertia of masses relatively to one another" [8].

The refinement of the understanding of inertia that Einstein left us with in relation to gravity, the Strong Equivalence Principle (SEP), only goes part-way in addressing Mach's principle. The SEP tells us that we can always remove the effects of gravity in a LIF in the neighbourhood of a point. However, it says nothing about the average effect of gravity, and therefore nothing about the "weighted average of the apparent motions" of the matter in the universe.

The question of what gravitational mass–energy is in general relativity is deeply subtle. On account of the SEP we can always get rid of gravity in the neighbourhood of a point, so any reasonable definition is necessarily quasilocal, involving integration over a bounding surface. The subject of quasilocal gravitational energy has occupied many mathematical relativists [88], and there is no universally agreed definition. This may reflect the fact that different notions of energy are applicable in different circumstances, just as in thermodynamics we deal with internal energy, and various free energies.

Two of the most familiar gravitational masses are the ADM mass [41] which is defined by an integral on a 2-sphere at spatial infinity for a general asymptotically flat spacetime, and the Komar mass [89, 90]

$$M = \frac{-c^2}{8\pi G}\int_{S^2_\infty} {}^*\mathrm{d}\mathbf{k} \tag{21}$$

which is similarly defined for asymptotically flat spacetimes with an asymptotically timelike Killing vector field, $\mathbf{k}$. The Komar mass is identical to that appearing in the Newtonian gravitational potential energy term, $\Phi = -GM/r$, in an asymptotic expansion, $g_{00} = -(1 + 2\Phi/c^2 + \ldots)$, at spatial infinity [90]. Most of the effort in the field of quasilocal gravitational energy has focused on ways of defining general geometrical energy quantities which reduce to familiar results in the case of isolated systems. Some interesting examples[12] include the definitions of Brown and York [91], and Epp [92]. With a few exceptions of quasilocal energies calculated in particular backgrounds, (e.g., [93]–[97]), very little has been done in a cosmological context, however.

For asymptotically flat geometries the average of the distribution of energy and momentum in the external universe is zero. In the actual universe the spacetime external to any concentrated mass also contains matter so that its geometry does not have a time symmetry but is necessarily dynamically evolving. In the timescape scenario it is proposed that in place of spatial infinity in (21) the mass definition for the largest bound structure should be made in reference to *finite infinity*, a timelike surface within which the average volume expansion is zero. In general there will be matter collapsing inwards around any virialized regions, and thus the finite infinity surface will be expanding at the boundary. (See Figure 1.) The density of a shell at the finite infinity surface defines the critical density. In a universe which is on average underdense there must always be such a transition zone between the overdense regions and the surrounding underdensity.

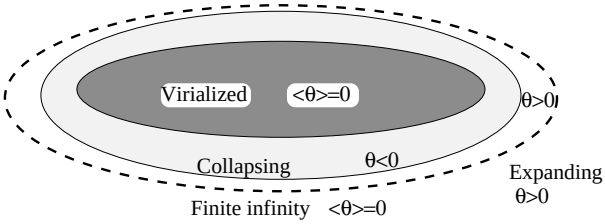

FIGURE 1. A schematic illustration of the notion of finite infinity, *fi* [13]: the boundary (dashed line) to a region with average zero expansion inside, and positive expansion outside.

Accounting for the average effect of matter to address Mach's principle effectively means specifying an appropriate definition of an asymptotic region, such as finite infinity, containing any local geometry. Local geometry should be determined by local matter, and if matter on a bounding sphere obeys some symmetry principle then we should look no further in determining the local standard of inertia. Since the very early universe started out being very close to spatially homogeneous and isotropic and cannot evolve arbitrarily far from from its initial conditions, it is proposed that such symmetries can always be found at a *regional* scale.

[12] This subject has a long history going back to Einstein, and a huge cast of mathematical relativists have made important contributions, which I will not attempt to summarize here. See ref. [88] for further details.

4.1. The cosmological equivalence principle

In the timescape scenario we restrict the geometry of expanding regions (the walls and voids) in the final stages of coarse-graining (2) to an average over domains which each obey the *cosmological equivalence principle* (CEP) [15]:

In cosmological averages it is always possible to choose a suitably defined spacetime region, the cosmological inertial region (CIR), on whose boundary average motions (timelike and null) can be described by geodesics in a geometry which is Minkowski up to some time-dependent conformal transformation,

$$\mathrm{d}s^2_{\rm CIR} = a^2(\eta)\left[-\mathrm{d}\eta^2 + \mathrm{d}r^2 + r^2\mathrm{d}{\Omega_2}^2\right]. \qquad (22)$$

A suitably defined region here refers to one which is smaller than the scalar curvature scale within underdense voids, or alternatively is the finite infinity scale for systems containing overdensities. Typically this could be of order $2\,h^{-1}$–$10\,h^{-1}$Mpc for finite infinity regions bounding small groups or rich clusters of galaxies.

Since the average geometry is a time–dependent conformal scaling of Minkowski space, the CEP reduces to the standard SEP if $a(\eta)$ is constant, or alternatively over very short time intervals during which the time variation of $a(\eta)$ can be neglected. It is well–known that for the exchange of photons between comoving observers in the background (22), to leading order the observed redshift of one comoving observer relative to another yields the same local Hubble law, whether the exact relation, $z+1 = a_0/a$, is used or alternatively the radial Doppler formula, $z+1 = [(c+v)/(c-v)]^{1/2}$, of special relativity is used, before making a local approximation. For a small spacetime region in a spatially homogeneous isotropic background this is a direct consequence of the SEP: it is impossible to distinguish whether particles are moving radially in a flat space, or alternatively are at rest in an expanding space.

The CEP makes the indistinguishability of radial motion from volume expansion a feature of regional averages on scales up to $2\,h^{-1}$–$10\,h^{-1}$Mpc, while allowing for inhomogeneity between this scale and the SHS. However, it disallows global coherent anisotropic expansion of the sort typified by Bianchi models. Bianchi models single out preferred directions in the global background universe, thereby imbuing spacetime with absolute qualities that go beyond an essentially relational structure. To make general relativity truly Machian such backgrounds need to be outlawed by principle, and the CEP achieves this while still allowing inhomogeneity.

The CIR metric (22) is of course the spatially flat FLRW metric, which in the standard cosmology is taken to be the geometry of the whole universe. In our case the whole universe is inhomogeneous subject to the restriction that it is possible to always choose (22) as a regional average in expanding regions.

4.2. Relative volume deceleration

To understand the physical implications of taking an average geometry (22) as the relevant average reference geometry for the relative calibration of rulers and clocks in the absence of global Killing vectors, let us construct a thought experiment analogy

that I will call the *semi-tethered lattice*. Take a lattice of observers in Minkowski space, initially moving isotropically away from each nearest neighbour at uniform initial velocities. The lattice of observers are chosen to be equidistant along mutually oriented $\hat{x}$, $\hat{y}$ and $\hat{z}$ axes. Suppose that the observers are each connected to six others by tethers of negligible mass and identical tension along the mutually oriented spatial axes. The tethers are not fixed but unwind freely from spools on which an arbitrarily long supply of tether is wound. The tethers initially unreel at the same uniform rate, representing a 'recession velocity'. Each observer carries synchronized clocks, and at a prearranged local proper time all observers apply brakes to each spool, the braking mechanisms having been preprogrammed to deliver the same impulse as a function of local time.

Applying brakes in the semi-tethered lattice experiment is directly analogous to the decelerating volume expansion of (22) due to some average homogeneous matter density, because it maintains the homogeneity and isotropy of space over a region as large as the lattice. Work is done in applying the brakes, and energy can be extracted from this – just as kinetic energy of expansion of the universe is converted to other forms by gravitational collapse. Since brakes are applied in unison, however, there is *no net force on any observer in the lattice*, justifying the *inertial frame* interpretation, even though each observer has a nonzero 4-acceleration with respect to the global Minkowski frame. The braking function may have an arbitrary time profile; provided it is applied uniformly at every lattice site the clocks will remain synchronous in the comoving sense, as all observers have undergone the same relative deceleration.

Whereas the Strong Equivalence Principle allows us to define local inertial frames, related to each other by local Lorentz transformations acting at a point, the Cosmological Equivalence Principle refers to a *collective* symmetry of the background. In defining the averaging region of the CIR we are isolating just that part of the volume expansion which is regionally homogeneous and isotropic.

Let us now consider two sets of disjoint semi-tethered lattices, with identical initial local expansion velocities, in a background static Minkowski space. (See Fig. 2(a).) Observers in the first congruence apply brakes in unison to decelerate homogeneously and isotropically at one rate. Observers in the second congruence do so similarly, but at a different rate. Suppose that when transformed to a global Minkowski frame, with time t, that at each time step the magnitudes of the 4–decelerations satisfy $\alpha_{_1}(t) > \alpha_{_2}(t)$ for the respective congruences. By special relativity, since members of the first congruence decelerate more than those of the second congruence, at any time t their proper times satisfy $\tau_{_1} < \tau_{_2}$. The members of the first congruence age less quickly than members of the second congruence.

By the CEP, the case of volume expansion of two disjoint regions of different average density in the actual universe is entirely analogous. The equivalence of the circumstance rests on the fact that by the evidence of the CMB the expansion of the universe was extremely uniform at the epoch of last scattering. At that time all regions had almost the *same* density – with tiny fluctuations – and the same uniform Hubble flow. At late epochs, suppose that in the frame of any average cosmological observer there are expanding regions of *different* density which have decelerated by different amounts by a given time, t, according to that observer. Then by the CEP the local proper time of the comoving observers in the denser region, which has decelerated more, will be less than that of the equivalent observers in the less dense region which has decelerated less. (See

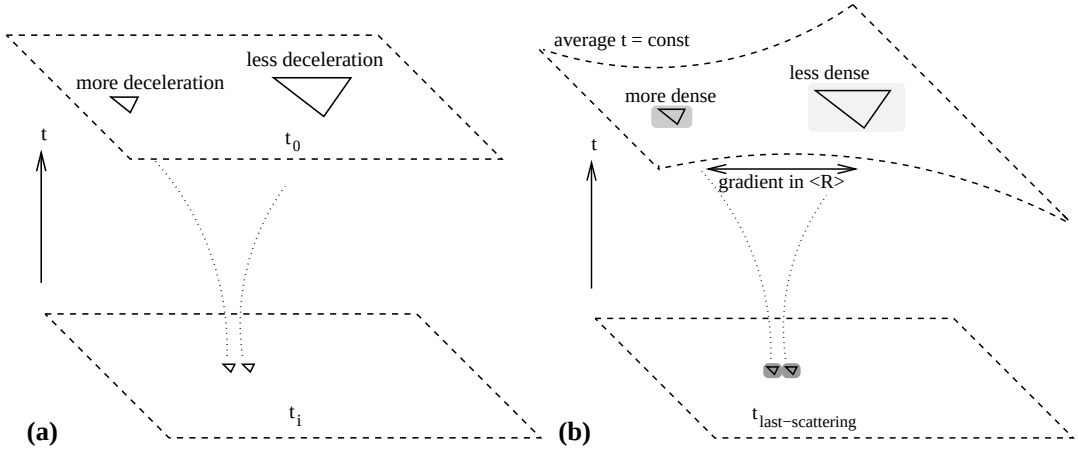

FIGURE 2. Two equivalent situations: **(a)** in Minkowski space observers in separate semi–tethered lattices, initially expanding at the same rate, apply brakes homogeneously and isotropically within their respective regions but at different rates; **(b)** in the universe which is close to homogeneous and isotropic at last-scattering comoving observers in separated regions initially move away from each other isotropically, but experience different locally homogeneous isotropic decelerations as local density contrasts grow. In both cases there is a relative deceleration of the observer congruences and those in the region which has decelerated more will age less.

Fig. 2(b).) Consequently the *proper time of the observers in the more dense CIR will be less than that of those in the less dense CIR*, by equivalence of the two situations.

The fact that a global Minkowski observer does not exist in the second case does not invalidate the argument. The global Minkowski time is just a coordinate label. In the cosmological case the only restriction is that the expansion of both average congruences must remain homogeneous and isotropic in local regions of different average density in the global average $t =$const slice. Provided we can patch the regional frames together suitably, then if regions in such a slice *are still expanding* and have a significant density contrast we can expect a significant clock rate variance.

This equivalence directly establishes the idea of a *gravitational energy cost for a spatial curvature gradient*, since the existence of expanding regions of different density within an average $t =$const slice implies a gradient in the average Ricci scalar curvature, $\langle \mathcal{R} \rangle$, on one hand, while the fact that the local proper time varies on account of the relative deceleration implies a gradient in gravitational energy on the other.

The variation of the normalization of asymptotic clocks due to a relative volume deceleration is a new physical effect. We are familiar with boosts in particular directions, which give significant effects only for large relative velocities; e.g., as required to remain stationary in strong gravitational fields. Since we only consider weak fields the relative deceleration of the background is small. However, even if the relative deceleration is typically of order $10^{-10}\mathrm{m\,s}^{-2}$, cumulatively over the age of the universe it leads to significant variation in the calibration of clocks, as we will discuss at the end of Sec. 5.2.

4.3. Statistical cosmological geometry

The timescape scenario represents an extension of the concepts of general relativity in the cosmological domain, as illustrated schematically in Fig. 3. In particular, it is recognized that once gravitational degrees of freedom are coarse–grained then one is no longer dealing with a simple solution of Einstein's equations with a prescribed matter source. Rather than cutting and pasting exact solutions of Einstein's equations as one does in the Swiss cheese [9] and meatball [57] models, we are dealing with a new statistical cosmological geometry in which the relative volume deceleration provides a physical degree of freedom to normalize canonical clocks. The relative phenomenological lapse function provides a measure of the relative kinetic energy of expansion of CIRs.

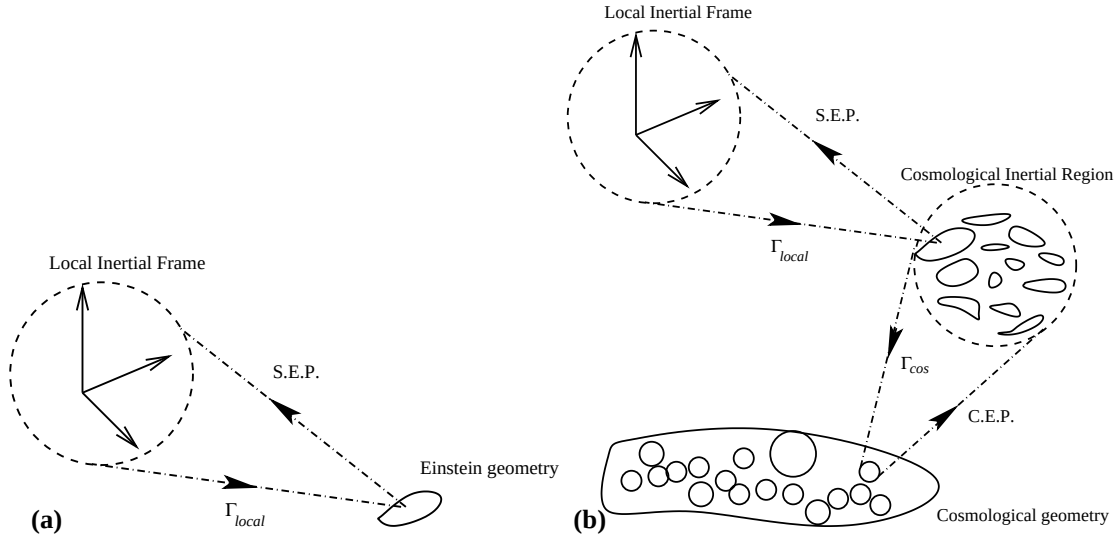

FIGURE 3. **(a)** In general relativity the SEP allows one to relate a solution of Einstein's equations with prescribed matter source to LIFs. The connection, Γ_{local}, allows one to parallely transport tensorial quantities from one LIF to another. **(b)** In the timescape scenario there is (at least) one additional layer of geometrical structure. Local geometries with asymptotic regions bounded by CIRs are combined in a cosmological average statistical geometry. The CEP allows one to relate a solution for the statistical geometry to the regional geometry of a CIR. The statistical cosmological geometry should be equipped with an appropriate connection, Γ_{cos}, to allow parallel transport from one CIR to another.

The Buchert formalism clearly deals with statistical quantities. However, although Buchert and Carfora [98] realized early on that there will be differences between the bare volume–average statistical parameters of the Buchert formalism and dressed parameters as determined by any particular observer, the relationship between observers and the statistical averages requires additional inputs and assumptions. Likewise one must specify what is understood by the phrase "comoving with the dust" once the dust approximation has broken down, as is the case for observers in gravitationally bound structures in overdense regions.

The timescape scenario seeks to address these questions by implementing the CEP. To date a rigorous geometrical framework for the statistical cosmological geometry has not been implemented. A phenomenological working framework will be outlined in the next section. Ultimately the geometrical framework should be one in which the Hubble parameter is to some extent a gauge choice – it corresponds to the first derivatives of

the metric of the statistical geometry encoded in the connection, Γ_{cos}. This is of course obvious in the early universe in which the FLRW and statistical geometry are one and the same, on account of global homogeneity and isotropy. How to develop an appropriate framework at late times is less obvious; however, it seems likely that should involve the notion of *scale invariance* of the statistical spatial 3-geometry.

5. TIMESCAPE SCENARIO: PHENOMENOLOGICAL MODEL

In order to deal with the evolution from the epoch of last scattering up to the present day, we assume that dust can be coarse-grained at the $\sim 100\,h^{-1}$Mpc scale of statistical homogeneity over which mass flows can be neglected. We apply the Buchert formalism, but interpret it in a different to Buchert [76, 77], who did not define the scale of coarse-graining of the dust explicitly. We will assumed that the Buchert average itself is performed over our present horizon volume, to describe average cosmic on the largest scales accessible to our observations.

Prior to last scattering the universe is close to homogeneous, so that timescape model is almost indistinguishable from the standard cosmology, being very close to a standard matter plus radiation FLRW model with negligible spatial curvature. At late epochs, the solutions to the Buchert equations will differ substantially from a FLRW model. Assuming no dark energy, then it is the matter density and its variance which drives the overall evolution of the universe. While the radiation fluid certainly responds to density gradients, this only affects questions such as gravitational lensing, rather than the average cosmological evolution described by the Buchert equations. We therefore treat the radiation fluid as a component with a pressure $P_{\rm R} = \frac{1}{3}\rho_{\rm R}$ which commutes under the Buchert average,

$$\partial_t \langle P_{\rm R}\rangle - \langle \partial_t P_{\rm R}\rangle = \langle P_{\rm R}\theta\rangle - \langle P_{\rm R}\rangle\langle\theta\rangle = 0, \tag{23}$$

throughout the evolution of the universe, rather than using the more detailed Buchert formalism that applies to fluids with pressure [77]. The relevant Buchert equations are then (13) with $\langle\rho\rangle \to \langle\rho_{\rm M}\rangle + \langle\rho_{\rm R}\rangle$, (14) with $\langle\rho\rangle \to \langle\rho_{\rm M}\rangle + 2\langle\rho_{\rm R}\rangle$, (15) with $\langle\rho\rangle \to \langle\rho_{\rm M}\rangle$, (19), and

$$\partial_t \langle\rho_{\rm R}\rangle + 4\frac{\dot{\bar{a}}}{\bar{a}}\langle\rho_{\rm R}\rangle = 0. \tag{24}$$

To obtain a phenomenologically realistic solution consistent with observations of voids in the cosmic web [2]–[4] we assume that the present epoch horizon volume, $\mathcal{V} = \mathcal{V}_{\rm i}\bar{a}^3$, is a disjoint union of void and wall regions characterized by scale factors $a_{\rm v}$ and $a_{\rm w}$ related to the volume-average scale factor by

$$\bar{a}^3 = f_{\rm vi}a_{\rm v}^{\ 3} + f_{\rm wi}a_{\rm w}^{\ 3} \tag{25}$$

where $f_{\rm vi}$ and $f_{\rm wi} = 1 - f_{\rm vi}$ represent the fraction of the initial volume, $\mathcal{V}_{\rm i}$, in void and wall regions respectively at an early unspecified epoch. We may rewrite (25) as

$$f_{\rm v}(t) + f_{\rm w}(t) = 1, \tag{26}$$

where $f_{\rm w}(t) = f_{\rm wi}{a_{\rm w}}^3/\bar{a}^3$ is the *wall volume fraction* and $f_{\rm v}(t) = f_{\rm vi}{a_{\rm v}}^3/\bar{a}^3$ is the *void volume fraction*. Taking a derivative of (25) with respect to the Buchert time parameter, t, we find that the bare Hubble parameter is given by

$$\bar{H} \equiv \frac{\dot{\bar{a}}}{\bar{a}} = f_{\rm w} H_{\rm w} + f_{\rm v} H_{\rm v}\,, \tag{27}$$

where $H_{\rm w} \equiv \dot{a_{\rm w}}/a_{\rm w}$ and $H_{\rm v} \equiv \dot{a_{\rm v}}/a_{\rm v}$ are the Hubble parameters of the walls and voids respectively as determined by the clocks of volume–average observers.

The voids are assumed to have negative spatial curvature characterized by $\langle\mathcal{R}\rangle_{\rm v} \equiv 6k_{\rm v}/{a_{\rm v}}^2$ with $k_{\rm v} < 0$, while the wall regions [13] are on average spatially flat, $\langle\mathcal{R}\rangle_{\rm w} = 0$. It then follows that

$$\langle\mathcal{R}\rangle = \frac{6k_{\rm v}{f_{\rm vi}}^{2/3}{f_{\rm v}}^{1/3}}{\bar{a}^2} \tag{28}$$

We also assume that the kinematic backreaction vanishes separately within the voids and walls[13] but not in the combined average. One then finds that the kinematic backreaction (16) reduces to a term depending on the relative expansion of voids and walls

$$\mathcal{Q} = 6f_{\rm v}(1-f_{\rm v})\left(H_{\rm v} - H_{\rm w}\right)^2 = \frac{2{\dot{f}_{\rm v}}^2}{3f_{\rm v}(1-f_{\rm v})}\,. \tag{29}$$

Since (15) and (24) are solved by $\langle\rho_{\rm M}\rangle = \bar{\rho}_{\rm M0}(\bar{a}/\bar{a}_0)^{-3}$ and $\langle\rho_{\rm R}\rangle = \bar{\rho}_{\rm R0}(\bar{a}/\bar{a}_0)^{-4}$ respectively, where the subscript zero refers to quantities evaluated at the present epoch, the remaining independent Buchert equations may then be written as

$$\frac{\dot{\bar{a}}^2}{\bar{a}^2} + \frac{{\dot{f}_{\rm v}}^2}{9f_{\rm v}(1-f_{\rm v})} - \frac{\alpha^2{f_{\rm v}}^{1/3}}{\bar{a}^2} = \frac{8\pi G}{3}\left(\bar{\rho}_{\rm M0}\frac{\bar{a}_0^3}{\bar{a}^3} + \bar{\rho}_{\rm R0}\frac{\bar{a}_0^4}{\bar{a}^4}\right), \tag{30}$$

$$\ddot{f}_{\rm v} + \frac{{\dot{f}_{\rm v}}^2(2f_{\rm v}-1)}{2f_{\rm v}(1-f_{\rm v})} + 3\frac{\dot{\bar{a}}}{\bar{a}}\dot{f}_{\rm v} - \frac{3\alpha^2{f_{\rm v}}^{1/3}(1-f_{\rm v})}{2\bar{a}^2} = 0, \tag{31}$$

where $\alpha^2 \equiv -k_{\rm v}{f_{\rm vi}}^{2/3} > 0$.

Equation (30) may also be conveniently written

$$\bar{\Omega}_M + \bar{\Omega}_R + \bar{\Omega}_k + \bar{\Omega}_{\mathcal{Q}} = 1, \tag{32}$$

---

[13] For spherical voids this is reasonable since the average shear and vorticity are small. Shear and vorticity may be significant within bound structures in the wall regions, but their contributions are of the opposite sign in the Raychaudhuri equation and might be largely self–canceling, giving rise to second order effects. The Buchert formalism neglects vorticity, and realistically this should be treated together with the effect of nonzero shear. Since we smooth at the finite infinity scale we are neglecting the gravitational physics associated with bound structures, where these effects are likely to be important. In the model presented here is assumed that the variation of the kinetic energy of expansion can be quantified independently of the gravitational physics within nonexpanding regions.

where

$$\bar{\Omega}_M \equiv \frac{8\pi G\bar{\rho}_{M0}\bar{a}_0^3}{3\bar{H}^2\bar{a}^3} \quad \bar{\Omega}_R \equiv \frac{8\pi G\bar{\rho}_{R0}\bar{a}_0^4}{3\bar{H}^2\bar{a}^4}, \quad \bar{\Omega}_k \equiv \frac{\alpha^2 {f_{\rm v}}^{1/3}}{\bar{a}^2\bar{H}^2}, \quad \bar{\Omega}_{\mathcal{Q}} \equiv \frac{-\dot{f}_{\rm v}^{\,2}}{9f_{\rm v}(1-f_{\rm v})\bar{H}^2}, \tag{33}$$

are the volume–average or *bare* density parameters [62, 98] of matter, radiation, average spatial curvature and kinematic backreaction respectively. It is straightforward to add a cosmological constant term to the r.h.s. of (30), giving rise to a further density parameter $\bar{\Omega}_\Lambda = \Lambda/(3\bar{H}^2)$, and in fact the equivalent solution with matter and a cosmological constant (but no radiation) has been derived in [99, 100]. Since we are interested in the possibility of a viable cosmology without dark energy, we set $\bar{\Omega}_\Lambda = 0$.

5.1. Matching regional to statistical geometry

Thus far we have simply set out the Buchert equations for a particular ensemble of wall and void regions, leading to differential equations which can be solved and possibly interpreted in many ways[14]. Since the Buchert equations describe statistical averages, the relationship of the statistical solutions to local geometry is crucial to the physical interpretation of the Buchert formalism. Here I will outline the phenomenological implementation of the principles of the timescape scenario discussed in Sec. 4.

The wall regions are a union of disjoint *finite infinity* regions [10, 13] encompassing bound structures, with local average metric (22), which can be rewritten as

$$\mathrm{d}s^2_{\mathcal{fi}} = -c^2\mathrm{d}\tau_{\rm w}^2 + {a_{\rm w}}^2(\tau_{\rm w})\left[\mathrm{d}\eta_{\rm w}^2 + \eta_{\rm w}^2\mathrm{d}{\Omega_2}^2\right]. \tag{34}$$

in terms of the wall time, $\tau_{\rm w}$, related to the wall conformal time by $c\,\mathrm{d}\tau_{\rm w} = a\,\mathrm{d}\eta_{\rm w}$. Although each finite infinity region is distinct, since they each represent a region within which the average density is critical, evolved from the same initial conditions, the $\tau_{\rm w}$ parameters can be taken to be synchronous.

The voids are characterized by regional negatively curved metrics of the form

$$\mathrm{d}s^2_{\mathcal{D}_{\rm v}} = -c^2\mathrm{d}\tau_{\rm v}^2 + {a_{\rm v}}^2(\tau_{\rm v})\left[\mathrm{d}\eta_{\rm v}^2 + \sinh^2(\eta_{\rm v})\mathrm{d}{\Omega_2}^2\right]. \tag{35}$$

Generally the voids will have different individual metrics (35). However, in the void centres the regional geometry will rapidly approach that of an empty Milne universe for which the parameters $\tau_{\rm v}$ can be assumed to be synchronous. One could potentially use different curvature scales for dominant voids and minivoids to characterize the average scalar curvature $\langle\mathcal{R}\rangle$. However, in the two–scale approximation of [13, 14] a single negative curvature scale is assumed as a simplification.

[14] Buchert and Carfora [101], and Wiegand and Buchert [102], have investigated a very similar model, without radiation, which also allows the possibility of internal kinematic backreaction within the walls and voids. They do not directly consider the issue of gravitational energy.

Within the dust particles the metrics (34) and (35) are assumed to be patched together with the condition of uniform quasilocal bare Hubble flow [13, 15]

$$\bar{H} = \frac{1}{a_{\rm w}}\frac{{\rm d}a_{\rm w}}{{\rm d}\tau_{\rm w}} = \frac{1}{a_{\rm v}}\frac{{\rm d}a_{\rm v}}{{\rm d}\tau_{\rm v}}, \tag{36}$$

discussed in Sec. 4.2. In particular, the regional Hubble parameters are also equal to the bare Buchert Hubble parameter (27). The Buchert average parameters $H_{\rm w}$ and $H_{\rm v}$ refer to expansion rates with respect to the volume–average time parameter t, so that (36) may be rewritten

$$\bar{H} = \bar{\gamma}_{\rm w} H_{\rm w} = \bar{\gamma}_{\rm v} H_{\rm v} \tag{37}$$

where

$$\bar{\gamma}_{\rm w} \equiv \frac{{\rm d}t}{{\rm d}\tau_{\rm w}}, \qquad \bar{\gamma}_{\rm v} \equiv \frac{{\rm d}t}{{\rm d}\tau_{\rm v}}, \tag{38}$$

are phenomenological lapse functions of volume–average time, t, relative to the time parameters of isotropic wall and void–centre observers respectively. The ratio of the relative Hubble rates $h_r = H_{\rm w}/H_{\rm v} < 1$ is related to the wall lapse function by

$$\bar{\gamma}_{\rm w} = 1 + \frac{(1-h_r)f_v}{h_r}, \tag{39}$$

and $\bar{\gamma}_{\rm v} = h_r \bar{\gamma}_{\rm w}$.

As we ourselves live in a bound structure and can be considered to be wall observers, there is no further need to refer to the void time parameter, $\tau_{\rm v}$. We will henceforth drop the subscript w from quantities defined in (38) and replace $\tau_{\rm w} \to \tau$, $\bar{\gamma}_{\rm w} \to \bar{\gamma}$.

We may rewrite $\bar{\Omega}_{\mathcal{Q}} = -(1-f_{\rm v})(1-\bar{\gamma})^2/(f_{\rm v}\bar{\gamma}^2)$, and combine it with the other density parameters (33) to give

$$\bar{\gamma} = \frac{\sqrt{1-f_{\rm v}}\left[\sqrt{1-f_{\rm v}} + \sqrt{f_{\rm v}(\bar{\Omega}-1)}\,\right]}{1-f_{\rm v}\bar{\Omega}}, \tag{40}$$

where

$$\bar{\Omega} \equiv 1 - \bar{\Omega}_{\mathcal{Q}} = \bar{\Omega}_M + \bar{\Omega}_R + \bar{\Omega}_k\,, \tag{41}$$

which satisfies $\bar{\Omega} > 1$ for the solutions of interest. As $t \to 0$, $f_{\rm v} \to 0$, $\bar{\Omega}_{\mathcal{Q}} \to 0$, $\bar{\Omega} \to 1$ and $\bar{\gamma} \to 1$; i.e., initially the void fraction and backreaction are negligible, and the wall time and volume-average time parameters coincide.

Solutions of the Buchert equations are not directly related to any physical metric. Since all cosmological information is obtained by a radial spherically symmetric null cone average, given a solution of the Buchert equations we will retrofit a spherically symmetric geometry relative to an isotropic observer who measures volume-average time, according to

$${\rm d}\bar{s}^2 = -c^2{\rm d}t^2 + \bar{a}^2(t)\,{\rm d}\bar{\eta}^2 + \mathcal{A}(\bar{\eta},t)\,{\rm d}{\Omega_2}^2. \tag{42}$$

Here the area quantity, $\mathcal{A}(\bar{\eta},t)$, satisfies $\int_0^{\bar{\eta}_{\mathcal{H}}} {\rm d}\bar{\eta}\,\mathcal{A}(\bar{\eta},t) = \bar{a}^2(t)\mathcal{V}_{\rm i}(\bar{\eta}_{\mathcal{H}})/(4\pi)$, $\bar{\eta}_{\mathcal{H}}$ being the conformal distance to the particle horizon relative to an observer at $\bar{\eta} = 0$. The metric

(42) is spherically symmetric by construction, but is not a LTB solution since it is not an exact solution of Einstein's equations, but rather a phenomenological fit to the Buchert average of the Einstein equations.

In terms of the wall time, τ, of finite infinity observers in walls the metric (42) is

$$\mathrm{d}\bar{s}^2 = -\bar{\gamma}^2(\tau)\, c^2\mathrm{d}\tau^2 + \bar{a}^2(\tau)\,\mathrm{d}\bar{\eta}^2 + \mathcal{A}(\bar{\eta},\tau)\,\mathrm{d}{\Omega_2}^2 . \tag{43}$$

This geometry, which has negative spatial curvature is not the locally measured geometry at finite infinity, which is given instead by (34). Since (34) is not a statistical geometry, we match (34) to (43) to obtain a *dressed* statistical geometry. The matching is achieved in two steps. Firstly we conformally match radial null geodesics of (34) and (43), noting that null geodesics are unaffected by an overall conformal scaling. This leads to a relation

$$\mathrm{d}\eta_{\mathrm{w}} = \frac{{f_{\mathrm{wi}}}^{1/3}\mathrm{d}\bar{\eta}}{\bar{\gamma}\,(1-f_{\mathrm{v}})^{1/3}} \tag{44}$$

along the geodesics. Secondly, we account for volume and area factors by taking η_{w} in (34) to be given by the integral of (44).

The wall geometry (34), which may also be written

$$\mathrm{d}s^2_{\mathcal{H}} = -c^2\mathrm{d}\tau^2 + \frac{(1-f_{\mathrm{v}})^{2/3}\,\bar{a}^2}{{f_{\mathrm{wi}}}^{2/3}}\left[\mathrm{d}\eta_{\mathrm{w}}^2 + \eta_{\mathrm{w}}^2\mathrm{d}{\Omega_2}^2\right] , \tag{45}$$

on account of (25), is a local geometry only valid in spatially flat wall regions. We now use (44) and its integral to extend this metric beyond the wall regions to obtain the dressed statistical metric

$$\begin{aligned}\mathrm{d}s^2 &= -c^2\mathrm{d}\tau^2 + \frac{\bar{a}^2}{\bar{\gamma}^2}\,\mathrm{d}\bar{\eta}^2 + \frac{\bar{a}^2\,(1-f_{\mathrm{v}})^{2/3}}{{f_{\mathrm{wi}}}^{2/3}}\,\eta_{\mathrm{w}}^2(\bar{\eta},\tau)\,\mathrm{d}{\Omega_2}^2 \\ &= -c^2\mathrm{d}\tau^2 + a^2(\tau)\left[\mathrm{d}\bar{\eta}^2 + r_{\mathrm{w}}^2(\bar{\eta},\tau)\,\mathrm{d}{\Omega_2}^2\right]\end{aligned} \tag{46}$$

where $a \equiv \bar{\gamma}^{-1}\bar{a}$, and

$$r_{\mathrm{w}} \equiv \bar{\gamma}\,(1-f_{\mathrm{v}})^{1/3}\,{f_{\mathrm{wi}}}^{-1/3}\eta_{\mathrm{w}}(\bar{\eta},\tau). \tag{47}$$

While (34) represents a local geometry only valid in spatially flat wall regions, the dressed geometry (46) represents an average effective geometry extended to the cosmological scales, parametrized by the volume–average conformal time which satisfies $\mathrm{d}\bar{\eta} = c\,\mathrm{d}t/\bar{a} = c\,\mathrm{d}\tau/a$. Since the geometry on cosmological scales does not have constant Gaussian curvature the average metric (46), like (42), is spherically symmetric but not homogeneous.

Wall observers who try to fit a FLRW model with 'cosmic time' synchronous to wall time, τ, are then effectively fitting the dressed geometry (46), which is the closest thing there is to a FLRW geometry adapted to the rulers and clocks of wall observers. The cosmological parameters we infer from taking averages on scales much larger than the SHS will not then be the bare parameters $\bar{H}$, $\bar{\Omega}_M$, $\bar{\Omega}_k$, and $\bar{\Omega}_{\mathcal{Q}}$, but instead the *dressed Hubble parameter*

$$H \equiv \frac{1}{a}\frac{\mathrm{d}a}{\mathrm{d}\tau} = \frac{1}{\bar{a}}\frac{\mathrm{d}\bar{a}}{\mathrm{d}\tau} - \frac{1}{\bar{\gamma}}\frac{\mathrm{d}\bar{\gamma}}{\mathrm{d}\tau} = \bar{\gamma}\bar{H} - \frac{\mathrm{d}\bar{\gamma}}{\mathrm{d}t}\,, \tag{48}$$

and the *dressed matter density parameter*

$$\Omega_{_M} = \bar{\gamma}^3 \bar{\Omega}_{_M} \,. \tag{49}$$

There is similarly a dressed luminosity distance relation

$$d_{_L} = a_0 (1+z) r_{\rm w}, \tag{50}$$

where $a_0 = \bar{a}_0/\bar{\gamma}_0$, $1+z \equiv a_0/a = (\bar{a}_0\bar{\gamma})/(\bar{a}\,\bar{\gamma}_0)$, and

$$r_{\rm w} = \bar{\gamma}_0 \, (1-f_{\rm v})^{1/3} \int_t^{t_0} \frac{c\,{\rm d}t'}{\bar{\gamma}(t')(1-f_{\rm v}(t'))^{1/3}\bar{a}(t')} \,, \tag{51}$$

We can also define an *effective angular diameter distance*, $d_{_A}$, and an *effective comoving distance*, D, to a redshift z in the standard fashion

$$d_{_A} = \frac{D}{1+z} = \frac{d_{_L}}{(1+z)^2} \,. \tag{52}$$

5.2. Cosmological solutions and their timescape interpretation

We have recently obtained [103] full numerical solutions of the Buchert equations for a matter plus radiation fluid, evolved forward from an early initial time when the solutions are well approximated by series solutions. E.g., we begin integrations after the epoch of primordial nucleosynthesis, at $\bar{H}_0 t \simeq 5 \times 10^{-11}$ when the universe is about a year old. Here $\bar{H}_0 = \bar{H}(t_0)$ is the bare (volume-average) Hubble constant. Bare density parameters (33) for typical solutions are shown in Fig. 4.

While numerical solutions are needed to smoothly match solutions from the radiation-dominated epoch to later epochs, the full numerical solution[15] possesses a tracking limit with a simple analytic form [14, 16] which is very accurate at epochs $z < 10$. The tracking corresponds to the walls expanding as an Einstein–de Sitter model, $a_{\rm w} = a_{\rm w0} t$, and the voids as an empty Milne universe, $a_{\rm v} = a_{\rm v0} t$, in volume average time, so that $h_r = 2/3$. The solution to the Buchert equations is then given by

$$\bar{a} \;=\; \frac{\bar{a}_0 (3\bar{H}_0 t)^{2/3}}{2+f_{\rm v0}} \Big[3 f_{\rm v0} \bar{H}_0 t + (1-f_{\rm v0})(2+f_{\rm v0}) \Big]^{1/3} \tag{53}$$

$$f_{\rm v} \;=\; \frac{3 f_{\rm v0} \bar{H}_0 t}{3 f_{\rm v0} \bar{H}_0 t + (1-f_{\rm v0})(2+f_{\rm v0})} \,. \tag{54}$$

The density parameters (33) and other quantities for the tracking solution are all found to have simple analytic forms in terms of the void fraction, $f_{\rm v}$. For example, the

[15] The matter only solution, $\bar{\Omega}_{_R} = 0$, is also analytically soluble [14, 16]. However, the tracking limit is reached to within 1% for redshifts $z \lesssim 37$. For larger redshifts $z \gtrsim 50$ one needs to include radiation to obtain accurate solutions. Thus the full numerical solution is actually required in that regime.

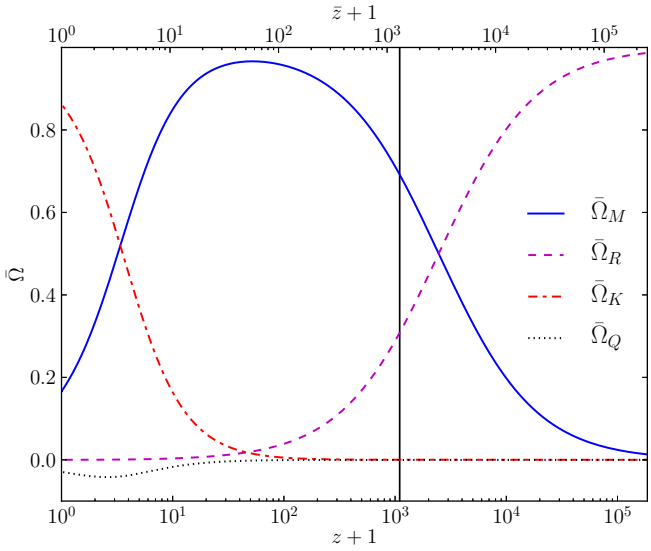

FIGURE 4. Bare density parameters (33) for the full numerical solution, as a function of dressed redshift $z+1=\bar{\gamma}\,\bar{a}_0/(\bar{\gamma}\,\bar{a})$ (and bare redshift $\bar{z}+1=\bar{a}_0/\bar{a}$), for the dressed parameters $H_0=61.7\,\mathrm{km\,s^{-1}\,Mpc^{-1}}$, $\Omega_{M0}=0.410$. The vertical bar at $1094.88<z<1100.46$ corresponds to the epoch of decoupling.

bare Hubble parameter, phenomenological lapse function, and dressed Hubble parameter satisfy $\bar{H}=(2+f_{\rm v})/(3t)$, $\bar{\gamma}=\frac{1}{2}(2+f_{\rm v})$ and $H=(4{f_{\rm v}}^2+f_{\rm v}+4)/(6t)$ respectively. (For further details, see ref. [16], Appendix B.) Parameters for the full numerical solution with radiation differ from those of the tracker solution by 0.3% or less at late times.

In the tracker limit the timescape wall time is related to volume average time by

$$\tau=\tfrac{2}{3}t+\frac{4\Omega_{M0}}{27f_{\rm v0}\bar{H}_0}\ln\left(1+\frac{9f_{\rm v0}\bar{H}_0t}{4\Omega_{M0}}\right), \tag{55}$$

where $\Omega_{M0}=\frac{1}{2}(1-f_{\rm v0})(2+f_{\rm v0})$ is the present epoch dressed matter density. In general the two parameters will differ substantially at late epochs – in fact by some billions of years – meaning that the age of the universe is observer–dependent. Nonetheless, we and all the objects we observe are necessarily in regions of greater than critical density, where the asymptotic time parameter is wall time, τ. Consequently this radical departure from conventional assumptions does not lead to any immediate conflict with observation, on account of our mass–biased view of the universe.

A present epoch large variation of clock rates, of order 35%, is the cumulative effect of an instantaneous relative volume deceleration between walls and voids which can be defined as [15]

$$\frac{\alpha}{c}=\frac{1}{\left[\bar{\gamma}^2-1\right]^{1/2}}\frac{\mathrm{d}\bar{\gamma}}{\mathrm{d}\tau}=\frac{\mathrm{d}}{\mathrm{d}t}\left[\bar{\gamma}^2-1\right]^{1/2}. \tag{56}$$

This is the deceleration that would arise from treating $\bar{\gamma}$ as the γ–factor of a purely transverse Lorentz boost. The phenomenological lapse function relates to an isotropic regional volume deceleration, and is not associated with any particular spatial direction,

which is why the transverse Lorentz boost formula is applied. For the late time tracker solution

$$\frac{\alpha}{c} = \frac{3(1-f_{\rm v0})(2+f_{\rm v0})f_{\rm v}(t)\bar{H}(t)}{2\sqrt{3f_{\rm v0}\bar{H}_0 t\left[15f_{\rm v0}\bar{H}_0 t + 4(1-f_{\rm v0})(2+f_{\rm v0})\right]}}\,. \tag{57}$$

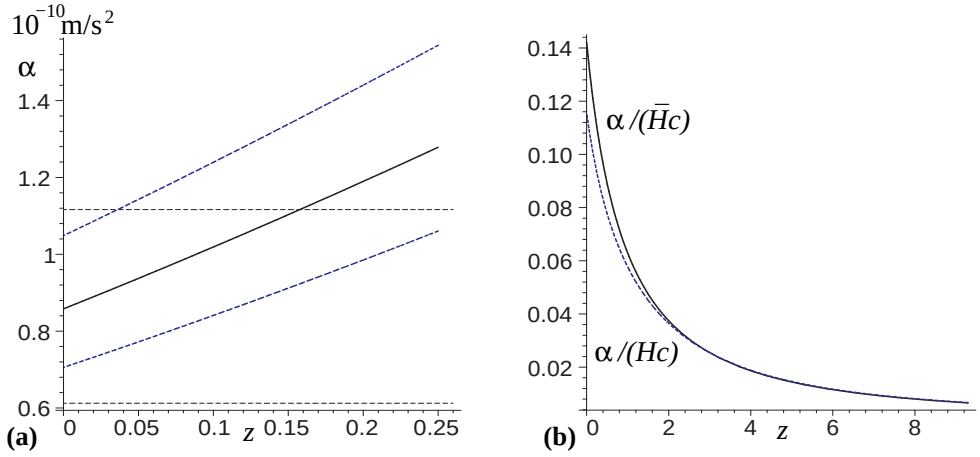

FIGURE 5. The magnitude of the relative deceleration scale [15], α: **(a)** in terms of its absolute value for redshifts $z < 0.25$; **(b)** in terms of the dimensionless ratios $\alpha/(c\bar{H})$ (solid curve) and $\alpha/(cH)$ (dashed curve) for redshifts $z < 10$. In panel (b) just the best fit value $f_{\rm v0} = 0.695$ is shown, whereas in panel (a) the solid and dashed represent the best fit value and 1σ uncertainties from Table 1. The narrower range of uncertainties obtained from the Planck data gives a smaller range of uncertainty in α as compared to earlier work [15]. In panel **(a)** the horizontal dotted lines indicate the upper and lower bounds of the empirical acceleration scale of MOND when normalized to $H_0 = 61.7 \pm 3.0\,{\rm km s^{-1}\,Mpc^{-1}}$.

The relative deceleration parameter is plotted in Fig. 5, in absolute terms at small redshifts, $z < 0.25$, and as a fraction of $c\bar{H}$ and cH over a larger range of redshifts. Although α is larger in absolute terms at earlier times, the Hubble expansion is much larger at early times, so that the ratio $\alpha/(c\bar{H})$ or $\alpha/(cH)$ is in fact small at large redshifts. Using the parameter values from Table 1 in Sec. 6.2, we find $\alpha_0 = 8.6^{+1.9}_{-1.5} \times 10^{-11}{\rm m\,s^{-2}}$ at $z = 0$, which is well within the weak field regime. Intriguingly, this coincides with the empirical acceleration scale of MOND, $\alpha_{\rm mond} = 1.2^{+0.3}_{-0.2} \times 10^{-10} h_{75}^2 {\rm ms^{-2}}$ [104], where $h_{75} = H_0/(75\,{\rm km s^{-1}\,Mpc^{-1}})$. For the values of H_0 given in Table 1, $\alpha_{\rm mond} = 8.1^{+3.0}_{-2.0} \times 10^{-11}{\rm ms^{-2}}$. It has been often observed that the value $\alpha_{\rm mond}$ is close to cH_0 [18]. However, cH_0 is actually one order of magnitude larger than $\alpha_{\rm mond}$, whereas here α_0 and $\alpha_{\rm mond}$ agree precisely within the uncertainty. Furthermore, α is a relative deceleration scale obtained from *derivatives* of quantities related to the Hubble parameter, meaning that one should not simply expect a numerical coincidence based on the value of H_0. Since the physics of bound systems has not been investigated in the timescape scenario, it remains to be seen whether the $\alpha_0 \simeq \alpha_{\rm mond}$ coincidence has any deeper significance.

5.3. Apparent acceleration and Hubble expansion variance

The gradient in gravitational energy and cumulative differences of clock rates between wall observers and volume average observers has an important consequence for apparent cosmic acceleration. A volume average isotropic observer, namely one whose local geometry has the same spatial curvature as the volume average, would infer an effective *bare deceleration parameter* $\bar{q} \equiv -\ddot{\bar{a}}/(\bar{H}^2\bar{a})$. Using the tracker solution approximation $\bar{q} = 2\,(1-f_{\rm v})^2/(2+f_{\rm v})^2$, which is always positive, meaning that there is no actual acceleration. However, a wall observer infers a *dressed deceleration parameter*

$$q = \frac{-1}{H^2 a}\frac{{\rm d}^2 a}{{\rm d}\tau^2} = \frac{-\,(1-f_{\rm v})\,(8{f_{\rm v}}^3+39{f_{\rm v}}^2-12f_{\rm v}-8)}{\left(4+f_{\rm v}+4{f_{\rm v}}^2\right)^2}\,, \tag{58}$$

where again we have used the tracker solution in the last step. At early times, when $f_{\rm v} \to 0$, both the bare and dressed deceleration parameters take the Einstein–de Sitter value $q \simeq \bar{q} \simeq \frac{1}{2}$. However, unlike the bare parameter which monotonically decreases to zero, the dressed parameter becomes negative when $f_{\rm v} \simeq 0.59$ and $\bar{q} \to 0^-$ at late times.

The origin of apparent cosmic acceleration in the timescape scenario differs from that envisaged in some other interpretations of the Buchert formalism, since $|\bar{\Omega}_{\mathcal{Q}}| \lesssim 0.042$ at all times which means that the backreaction is never large enough to make $\bar{q}$ negative. Cosmic acceleration is recognized as an apparent effect which arises due to the cumulative clock rate variance of wall observers relative to volume–average observers. It becomes significant only when the voids begin to dominate the universe by volume, which occurs at low redshifts. Since the epoch of onset of apparent acceleration is directly related to the void fraction, $f_{\rm v}$, this solves the cosmic coincidence problem.

In addition to apparent cosmic acceleration, another important apparent effect will arise if one considers scales below the SHS. By any one set of clocks it will appear that voids expand faster than wall regions. Thus a wall observer will see galaxies on the far side of a dominant void of diameter $\sim 30\,h^{-1}$Mpc to have a greater local Hubble parameter than the dressed global average H_0, while galaxies within an ideal wall have a local Hubble parameter lower than H_0. The local maximum Hubble parameter across a void seen by a wall observer is $H_{\rm vw0} = \frac{1}{a_{\rm v}}\frac{{\rm d}a_{\rm v}}{{\rm d}\tau} = h_r^{-1}\bar{H} \simeq \frac{3}{2}\bar{H}$. Furthermore, since the bare Hubble parameter $\bar{H}$ provides a measure of the uniform quasilocal flow, it must also be the minimum 'local' value within an ideal wall at any epoch. With a dressed Hubble constant $H_0 = 61.7 \pm 3.0\,{\rm km\,s^{-1}\,Mpc^{-1}}$ (see Table 1), we can expect a local Hubble expansion that varies between a minimum $50.1 \pm 1.7\,{\rm km\,s^{-1}\,Mpc^{-1}}$ within our local filament (towards the Virgo cluster), and a maximum $75.2^{+2.0}_{-2.6}\,{\rm km\,s^{-1}\,Mpc^{-1}}$ across local voids. Averaging over many structures in spherical shells will reduce the variation, as will be discussed in Sec. 7.

6. TIMESCAPE SCENARIO: OBSERVATIONAL TESTS

There are three types of potential cosmological tests of the timescape scenario:

(i) tests of the average expansion history on scales larger than the SHS, involving quantities derived from luminosity and angular diameter distance measures;

(ii) tests of cosmological averages on scales larger than the SHS that include contributions from the growth of structures (late epoch integrated Sachs–Wolfe effect, cosmic shear, weak lensing, redshift space distortions etc);

(iii) tests of the local expansion history below the SHS.

Class (iii) deals with scales which are in the nonlinear regime of perturbation theory in the standard model, and it is quite possible that this regime needs to be understood before one can make progress with class (ii). Tests in class (i) will include equivalents to every cosmological test of the standard FLRW model. We will consider class (i) tests in Secs. 6.1–6.3, 6.6; tests which require the treatment of redshift space distortions and therefore fall into class (ii) in Secs. 6.4, 6.5; and finally a class (iii) test in Sec. 7.

6.1. Luminosity distances: supernovae, gamma ray bursts

The luminosity distance relations (50), (51) have been tested extensively with type Ia supernovae (SneIa) data [105, 106] and with gamma–ray bursters [107]. In the case of the supernovae, it turns out that the luminosity distance is so close to that of the standard model that the question of whether a better fit is provided by the timescape model or by the spatially flat ΛCDM model depends on the manner in which the data is reduced [106]. In other words, the differences between the two models are at the level of current systematic uncertainties in SneIa data reduction – supernovae being standardizable candles, rather than perfect standard candles.

Two empirical methods commonly used to reduce SNeIa data are the Multicolor Light Curve Shape fitter MLCS2k2 [108], and the Spectral Adaptive Light curve Template SALT/SALT-II methods [109, 110]. MLCS2k2 calibration uses a nearby training set of SNeIa assuming a close to linear Hubble law, whereas SALT/SALT-II uses the whole dataset to calibrate empirical light curve parameters. Since SneIa from beyond the range in which the Hubble law is linear are used, a cosmological model must be assumed[16]. We find that the timescape model provides a better fit to SneIa data than the standard spatially flat ΛCDM model if the MLCS2k2 method is used, while conversely the standard model provides a better fit if the SALT-II method is used [106]. However, the

[16] In refs. [111, 112] it is incorrectly stated that in the SALT/SALT-II methods data is reduced "assuming the Friedmann equation". In fact, any cosmological model can be used in applying the SALT/SALT-II method, and in ref. [106] we have applied it to the timescape model. However, it is true that *very often* data is reduced using the standard cosmology with the Friedmann equation to produce tables of apparent magnitudes and redshifts. Data reduced in this fashion cannot be used to test non-standard cosmologies; one must perform a separate SALT/SALT-II data reduction for each nonstandard model that one investigates.

Bayesian evidence for these conclusions is not very strong.

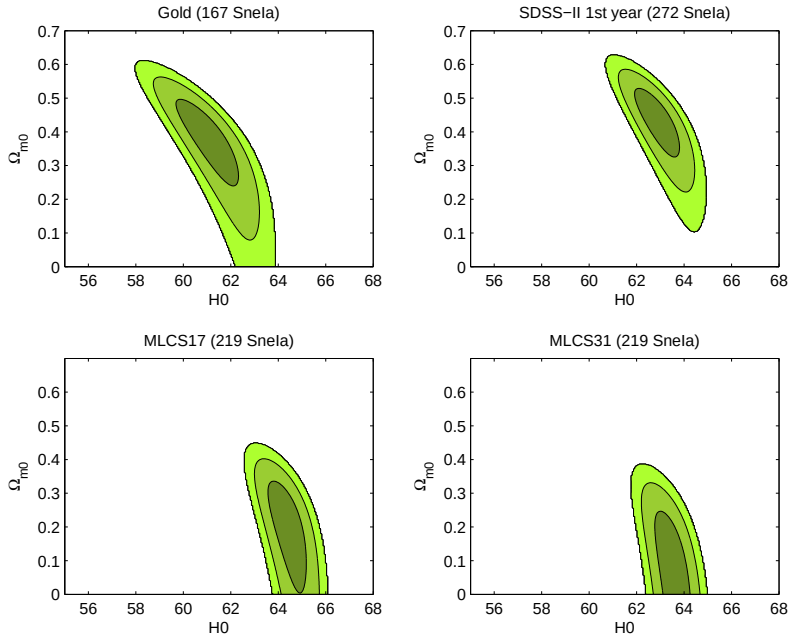

FIGURE 6. Confidence limits [106] for timescape model fits to $z \geq 0.033$ cut samples of Gold07 ($R_V = 3.1$) [113], SDSS-II ($R_V = 2.18$) [114], MLCS17 ($R_V = 1.7$) and MLCS31 ($R_V = 3.1$) [115]. In each case an overall normalization of the Hubble constant from the published dataset is assumed.

One important issue that arises in the timescape model is that the luminosity distance relation (50), (51) only applies on scales larger than the SHS. In some SneIa compilations data below this scale is included. Such data needs to be removed when testing the timescape model. It was found that even when such systematics are accounted for, there are still marked differences in the cosmological parameters deduced[17] depending on additional assumptions made in data reduction, as is seen in Fig. 6 in which 4 different implementations of MLCS2k2 are considered. There is a known degeneracy between intrinsic colour variations in SneIa and reddening by dust in the host galaxy, determined by the parameter R_V. However, the differences seen between the different panels in Fig. 6 involve more than simply the value of this parameter. Much remains to be done to resolve these systematic issues.

In recent years correlations of empirical properties of gamma-ray bursters have been used to determine Hubble diagrams at larger redshifts than those probed by SneIa [116]–[119]. A recent analysis of 69 GRBs [107] found that the timescape model gave a better fit than the spatially flat ΛCDM model, but not by a margin that is statistically significant. Further improvement in understanding of the systematic issues is required before GRB can provide tight constraints.

[17] It should be noted that in the MLCS method the value of H_0 depends on an overall calibration of the distance scale; e.g., from Cepheid distances. There is therefore a freedom to shift the contours along the H_0 axis in Fig. 6 depending on that normalization. The relative value of H_0 for different fits is more important than the absolute values.

6.2. Cosmic microwave background anisotropies

A complete analysis of the CMB anisotropy spectrum in the timescape cosmology is highly nontrivial, since the standard model analysis includes the late time integrated Sachs-Wolfe effect, which requires a from first principles reinvestigation in the timescape model. While such an analysis has not yet been completed, we are nonetheless able to compute the angular diameter distance of the sound horizon at any epoch, and to independently compute the epochs of matter–radiation decoupling, photon–electron decoupling and the baryon drag epoch, and substantial constraints on model parameters [103] can already be made using the Planck data [1].

Since the early universe is extremely close to being spatially homogeneous and isotropic, in the timescape model there is no change to physical processes at those epochs, but rather in the calibration of parameters. In our case, there are two sets of observers – wall observers such as ourselves, and the volume average observers to whom the average cosmological parameters (33) are most directly related. Computations are most readily performed from the point of view of the volume-average observers, if we account for the fact that they determine a cooler CMB temperature than us at the present epoch. There is a focusing and defocusing of light between walls and voids, and the number density of CMB photons in the negatively curved voids is less than in the walls.

The volume-average CMB temperature, $\bar{T}$, is related to wall temperature, T, by

$$\bar{T} = \bar{\gamma}^{-1} T \,, \tag{59}$$

at any epoch. The difference is negligible at early times when $\bar{\gamma} \simeq 1$; however, at the present epoch $\bar{T}_0 = \bar{\gamma}_0^{-1} 2.275\,\mathrm{K}$ is typically 35% lower than the temperature we measure. The bare baryon number density is then given by

$$\bar{n}_{\rm B} = \frac{3\bar{H}_0^2 \bar{\Omega}_{\rm B0}}{8\pi G m_{\rm p}} \left(\frac{\bar{T}}{\bar{T}_0} \right)^3 \,, \tag{60}$$

where $\bar{\Omega}_{\rm B0}$ is the present epoch bare baryon matter density parameter and $m_{\rm p}$ is the proton mass.

The standard analysis of early universe physics applies when calibrated in terms of volume-average parameters. One very important consequence of this is that the baryon–to–photon ratio, $\eta_{B\gamma}$, is recalibrated as compared to the standard cosmology, and we can potentially obtain a fit with no primordial lithium abundance anomaly [120]. In particular, timescape fits have been performed [13, 103, 105] for the range $\eta_{B\gamma} = (5.1 \pm 0.5) \times 10^{-10}$ favoured by constraints from light element abundances alone[18] [121, 122].

[18] A higher value is assumed in ΛCDM fits of CMB data, giving rise to the lithium abundance anomaly. While there is an intrinsic tension in the light element data between abundances of deuterium and lithium-7 [122], for the range of $\eta_{B\gamma}$ we adopt here all abundances fall within 2σ.

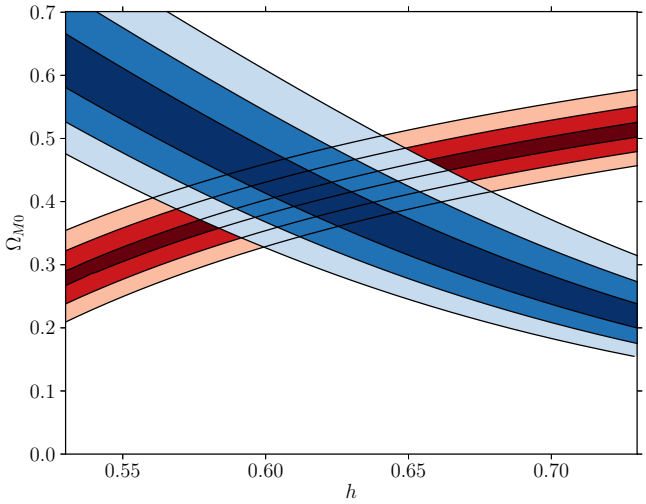

FIGURE 7. Contours of (h, Ω_{M0}) parameter values for which the angular diameter of the sound horizon at decoupling matches the angular scale $\theta_* = 0.0104139$ [1] to within $\pm 2\%$, $\pm 4\%$ and $\pm 6\%$ are shown in blue (upper left to lower right). Contours of parameter values for which the present-day effective comoving scale of the sound horizon at the baryon drag epoch matches the value $98.88\,h^{-1}$Mpc [1] are shown in red (lower left to upper right). In each case the baryon–to–photon ratio is assumed to be in the range $4.6 < 10^{10}\eta_{B\gamma} < 5.6$, for which there is no primordial lithium abundance anomaly [120].

The volume–average sound horizon scale at any epoch is given by

$$\bar{D}_s = \frac{\bar{a}(t)}{\bar{a}_0}\frac{c}{\sqrt{3}}\int_0^{x_{\rm dec}} \frac{{\rm d}x}{x^2\bar{H}\sqrt{1+0.75\,x\,\bar{\Omega}_{\rm B0}/\bar{\Omega}_{\gamma 0}}}, \tag{61}$$

where $\bar{\Omega}_{\gamma 0} = 2g_*^{-1}\bar{\Omega}_{\rm R0}$ is the present epoch volume-average photon density parameter, $g_* = 3.36$ is the relative degeneracy factor of relativistic species, $x_{\rm dec} = \bar{z}_{\rm dec} + 1 \equiv \bar{\gamma}_0(1+z_{\rm dec})/\bar{\gamma}_{\rm dec}$ is the value of $\bar{a}/\bar{a}_0$ at photon–electron decoupling, and $\bar{\Omega}_{\rm B0} = \eta_{B\gamma} m_{\rm p}\bar{n}_{\gamma 0}$ is fixed in terms of $m_{\rm p}$, $\eta_{B\gamma}$ and the present epoch volume–average photon density, $\bar{n}_{\gamma 0}$.

We compute the comoving scale of the sound horizon at photon– electron decoupling, $\bar{D}_s(t_{\rm dec})$, from (61), and its angular diameter distance, $d_{A\,\rm dec}$, from (50)–(52) using the numerical solutions to (30), (31) at the same time as solving the Peebles equation to determine the ionization fraction [103]. The angular scale $\theta_* = \bar{D}_s(t_{\rm dec})/d_{A\,\rm dec}$ can then be constrained to match the measured value [1] to any desired accuracy.

For BAO measurements, the relevant comoving size of the sound horizon is that at the baryon drag epoch, which occurs at $t = t_{\rm drag}$ when $c\tau_{\rm d} \simeq 1$, where

$$\tau_{\rm d}(t) \equiv \int_t^{t_0} \frac{\dot{\tau}_{\rm o}\,{\rm d}t}{\bar{a}R} = \int_t^{t_0} \frac{\sigma_{\rm T}\bar{n}_{\rm e}\,{\rm d}t}{\bar{a}R} \tag{62}$$

is the drag depth, $\tau_{\rm o}$ is the optical depth, $\sigma_{\rm T}$ is the Thomson scattering cross-section, $\bar{n}_{\rm e} = \bar{n}_{\rm p}$ is the bare free electron density, and $R \equiv 0.75\rho_B/\rho_\gamma = 0.75\,(\bar{\Omega}_{\rm B0}\bar{a})/(\bar{\Omega}_{\gamma 0}\bar{a}_0)$. Since we are not yet able to constrain the BAO scale directly from galaxy clustering

TABLE 1. Estimates of the cosmological parameters of the timescape model [103] obtained from a $\pm 2\%$ match to the angular scale, θ_*, of the sound horizon at decoupling; and to a $\pm 6\%$ match to the effective comoving scale, $r_{\rm drag}$, of the sound horizon at the baryon drag epoch, using recent values from the Planck satellite analysis [1]. A tighter constraint is applied to θ_* as it is purely geometrical, whereas the calibration of $r_{\rm drag}$ involves additional uncertainty since the ratio of nonbaryonic to baryonic matter densities may differ between the timescape and ΛCDM models.

Parameter		Range
Present void fraction	$f_{\rm v0}$	$0.695^{+0.041}_{-0.051}$
Bare Hubble constant	$\bar{H}_0$	$50.1 \pm 1.7\,{\rm km s^{-1}\,Mpc^{-1}}$
Dressed Hubble constant	H_0	$61.7 \pm 3.0\,{\rm km s^{-1}\,Mpc^{-1}}$
Local maximum Hubble constant	$H_{\rm vw0}$	$75.2^{+2.0}_{-2.6}\,{\rm km s^{-1}\,Mpc^{-1}}$
Present phenomenological lapse function	$\bar{\gamma}_{_0}$	$1.348^{+0.021}_{-0.025}$
Dressed matter density parameter	Ω_{M0}	$0.41^{+0.06}_{-0.05}$
Dressed baryon density parameter	Ω_{B0}	$0.074^{+0.013}_{-0.011}$
Bare matter density parameter	$\bar{\Omega}_{M0}$	$0.167^{+0.036}_{-0.037}$
Bare baryon density parameter	$\bar{\Omega}_{\rm B0}$	$0.030^{+0.007}_{-0.005}$
Bare radiation density parameter	$\bar{\Omega}_{\rm R0}$	$\left(5.00^{+0.56}_{-0.48}\right) \times 10^{-5}$
Bare curvature parameter	$\bar{\Omega}_{\rm k0}$	$0.862^{+0.024}_{-0.032}$
Bare backreaction parameter	$\bar{\Omega}_{\mathcal{Q}0}$	$-0.0293^{+0.0033}_{-0.0036}$
Nonbaryonic/baryonic matter densities ratio	$\bar{\Omega}_{\rm C0}/\bar{\Omega}_{\rm B0}$	$4.6^{+2.5}_{-2.1}$
Age of universe (galaxy/wall observer)	τ_0	$14.2 \pm 0.5\,{\rm Gyr}$
Age of universe (volume-average observer)	$t_{_0}$	$17.5 \pm 0.6\,{\rm Gyr}$
Apparent acceleration onset redshift	$z_{\rm acc}$	$0.46^{+0.26}_{-0.25}$

statistics, we determine $\bar{D}_s(t_{\rm drag})$ at the same time as other numerical integrations, and constrain it using Planck satellite estimates [1].

In Fig. 7 we display two sets of contours in the (H_0, Ω_{M0}) parameter space obtained in ref. [103]: firstly, parameters which match the acoustic scale of the sound horizon $\theta_* = 0.0104139$ [1] to within $\pm 2\%$, $\pm 4\%$ or $\pm 6\%$; and secondly parameters which similarly match the present effective comoving scale of the sound horizon at the baryon drag epoch as determined by the standard ΛCDM model analysis of the Planck data, namely[19] $98.88\,h^{-1}$Mpc [1].

The full numerical solutions [103] provide tighter constraints than earlier analyses [105], leading to the parameters listed[20] in Table 1. Particular parameters can be ruled out on the basis that matter–radiation equality must occur before last scattering, so that $\bar{\Omega}_M/\bar{\Omega}_R > 1$ at $z_{\rm dec}$. In particular, we can rule out a dressed matter density parameter

[19] Since the Hubble constant $H_0 = 67.11\,{\rm km s^{-1}\,Mpc^{-1}}$ determined from the Planck satellite is a fit to the ΛCDM model, any effective present comoving scale must be given in units h^{-1}Mpc, as the timescape model will generally yield a different value for H_0.

[20] A recent phenomenologically motivated analysis [123] using a completely different approach produces a void fraction which agrees with that found here.

$\Omega_{M0} < 0.2$ if $H_0 < 65\,\mathrm{km\,s^{-1}\,Mpc^{-1}}$. If we compare Fig. 6 we see that the SneIa data reduction methods used in the Gold07 [113] and SDSS-II [114] samples remain consistent with the new constraints, whereas those of ref. [115] do not.

A detailed treatment of the acoustic peaks in the CMB data may of course still challenge the timescape cosmology, as it will certainly further tighten the constraints. Work on this problem, which requires a revisiting of CMB data analysis from first principles, is in progress.

6.3. The effective 'equation of state'

A direct method for comparing the expansion history with those of homogeneous models with dark energy, is to observe that for a standard spatially flat cosmology with dark energy obeying an equation of state $P_{\mathcal{D}} = w(z)\rho_{\mathcal{D}}$, the quantity

$$\frac{H_0 D}{c} = \int_0^z \frac{\mathrm{d}z'}{\left[\Omega_{M0}(1+z')^3 + \Omega_{D0}\exp\left(3\int_0^{z'}\frac{(1+w(z''))\mathrm{d}z''}{1+z''}\right)\right]^{1/2}}\,, \tag{63}$$

does not depend on the value of the Hubble constant, H_0, but only directly on $\Omega_{M0} = 1 - \Omega_{D0}$. Since the best-fit values of H_0 are potentially different for different models, a comparison of $H_0 D/c$ curves as a function of redshift for the timescape model versus the ΛCDM model gives a good indication of where the largest differences can be expected, independently of the value of H_0. Such a comparison is made in Fig. 8.

As the redshift range changes the timescape model interpolates between ΛCDM models with different values of (Ω_{M0},$\Omega_{\Lambda 0}$). If we consider the timescape model that is a best fit to the Planck data, then for the largest redshifts $50 \lesssim z \lesssim 1100$, D_{TS} is essentially indistinguishable from the $D_{\Lambda\mathrm{CDM}}$ for model (i) with parameter values $(\Omega_{M0}, \Omega_{\Lambda 0}) = (0.3175, 0.6825)$ which best-fit the Planck data [1]. By contrast over the range $2 \lesssim z \lesssim 6$ a close fit is provided by model (ii) with $(\Omega_{M0}, \Omega_{\Lambda 0}) = (0.35, 0.65)$. For the closest redshifts, $z < 1.5$, D_{TS} becomes indistinguishable from $D_{\Lambda\mathrm{CDM}}$ for model (iii) with $(\Omega_{M0}, \Omega_{\Lambda 0}) = (0.338, 0.721)$. It is this feature which makes it difficult to distinguish the timescape model from the ΛCDM model on the basis of SneIa data alone. However, with complementary tests over the full range of redshifts the expansion histories should be distinguishable.

Fig. 8 shows just one value of $f_{\mathrm{v}0}$. If we compare Fig. 2 of Ref. [16], we see that with $f_{\mathrm{v}0} = 0.76$, D_{TS} similarly interpolates between ΛCDM models with $(\Omega_{M0}, \Omega_{\Lambda 0}) = (0.34, 0.64)$ at low redshift and $(\Omega_{M0}, \Omega_{\Lambda 0}) = (0.25, 0.75)$ at high redshift. I.e., as the present epoch void fraction is increased the width of the range of equivalent ΛCDM Ω_{M0} values increases, as well as the overall values being less.

The shapes of the $H_0 D/c$ curves depicted in Fig. 8 represent the actual observable quantity one is measuring in tests that some researchers loosely refer to as 'measuring the equation of state'. For spatially flat dark energy models, with $H_0 D/c$ given by (63), one finds that the function $w(z)$ appearing in the fluid equation of state $P_{\mathcal{D}} = w(z)\rho_{\mathcal{D}}$ is

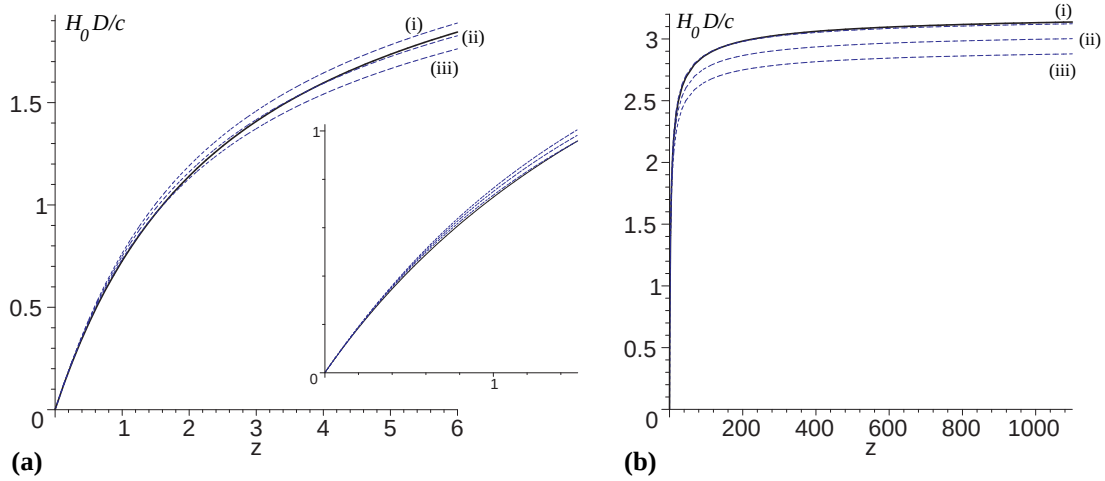

FIGURE 8. The effective comoving distance $c^{-1}H_0D(z)$ is plotted for the timescape model which best fits Planck [1], with $f_{\rm v0} = 0.695$ (solid line) [103]; and for various spatially flat ΛCDM models (dashed lines). The parameters for the dashed lines are (i) $\Omega_{M0} = 0.3175$ (best-fit ΛCDM model to Planck [1]); (ii) $\Omega_{M0} = 0.35$; (iii) $\Omega_{M0} = 0.388$. Panel **(a)** shows the redshift range $z < 6$, with an inset for $z < 1.5$, which is the range tested by SneIa data. Panel **(b)** shows the range $z < 1100$ to the surface of last scattering, tested by Planck.

related to the first and second derivatives of (63) by

$$w(z) = \frac{\frac{2}{3}(1+z)D'^{-1}D'' + 1}{\Omega_{M0}(1+z)^3 H_0^2 D'^2 c^{-2} - 1} \tag{64}$$

where prime denotes a derivative with respect to z. Such a relation can be applied to observed distance measurements, regardless of whether the underlying cosmology has dark energy or not. Since it involves first and second derivatives of the observed quantities, it is actually much more difficult to determine observationally than directly fitting $c^{-1}H_0D(z)$.

The equivalent of the equation of state, $w(z)$, for the timescape model is plotted in Fig. 9. The fact that $w(z)$ is undefined at a particular redshift and changes sign through $\pm\infty$ simply reflects the fact that in (64) we are dividing by a quantity which goes to zero for the timescape model, even though the underlying curve of Fig. 8 is smooth. As we are not dealing with a dark energy fluid in the timescape model, $w(z)$ simply has no physical meaning.

Nonetheless, phenomenologically the results do agree with the usual inferences about $w(z)$ for fits of standard dark energy cosmologies to SneIa data. In particular, for low redshifts the average value of $w(z)$ is close to -1, but it eventually it crosses 'the phantom divide' to $w(z) < -1$. For fundamental homogeneous dark energy fluids, $w < -1$ signals a violation of the dominant energy condition and with that a breakdown of standard laws of physics. Here it is simply a consequence of an inappropriate parametrization of the expansion history of a universe which does not evolve according to the Friedmann equation.

The redshift at which '$w = -1$ is crossed' in the timescape model depends on the value of Ω_{M0} that is assumed in the FLRW style analysis. For the canonical model

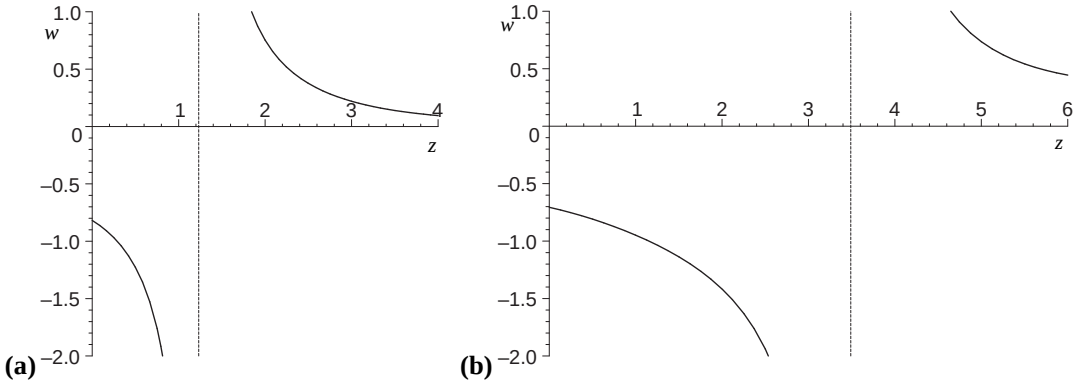

FIGURE 9. The artificial equivalent of an equation of state constructed using the effective comoving distance (64), plotted for the timescape tracker solution with best-fit value $f_{\rm v0} = 0.695$, and two different values of Ω_{M0}: **(a)** the canonical dressed value $\Omega_{M0} = \frac{1}{2}(1 - f_{\rm v0})(2 + f_{\rm v0}) = 0.41$; **(b)** $\Omega_{M0} = 0.3175$.

of Fig. 9(a), with $\Omega_{M0} = 0.41$ one finds that '$w = -1$ is crossed' at $z = 0.29$, with $\Omega_{M0} = 0.388$ '$w = -1$ is crossed' at $z = 0.40$, and with $\Omega_{M0} = 0.3175$ (the ΛCDM value from Planck [1] in Fig. 9(b)), '$w = -1$ is crossed' at $z = 1.15$. For the same value of $f_{\rm v0}$, taking a lower value of Ω_{M0} in a FLRW–style analysis leads to $w(z)$ being closer to $w = -1$ for a larger range of redshifts. Thus if a timescape model luminosity distance relation is correct then one can easily be led to different conclusions about 'dynamical dark energy' [124, 125] over the range of redshifts, $z < 1.5$, probed by SneIa, depending on prior assumptions about the value of Ω_{M0} from other datasets.

What appears as an Ω_{M0} dependent varying $w(z)$ from the FLRW perspective actually reflects the fact that the effective energy density assumed in the standard analysis is not scaling as $\bar{\Omega}_M \propto (1+z)^3$, as would be the case for any homogeneous model. Consequently the timescape model simply lies outside the class of models typically contemplated for dark energy diagnostics [126]–[128]. For example, the $Om(z)$ diagnostic of Sahni, Shafieloo and Starobinsky [128, 129] is designed to be a constant, Ω_{M0}, at all redshifts for a spatially flat FLRW model, but to differ for other $w(z)$ functions. One can compute a formula for the $Om(z)$ diagnostic [16], although this is not particularly useful since the timescape model has a singular $w(z)$ and lies outside the class of empirical functions usually used to analyse the diagnostic. Existing analyses can only be applied in asymptotic limits such as $z \to 0$, when [16]

$$Om(0) = \tfrac{2}{3}\, H'|_0 = \frac{2(8f_{\rm v0}^3 - 3f_{\rm v0}^2 + 4)(2 + f_{\rm v0})}{(4f_{\rm v0}^2 + f_{\rm v0} + 4)^2} \qquad (65)$$

For $f_{\rm v0} = 0.695^{+0.041}_{-0.051}$, $Om(0) = 0.643^{+0.008}_{-0.004}$. In fact, this coincides with the intercept of Fig. 3 in ref. [129], determined from SneIa, BAO and CMB data.

6.4. The Alcock–Paczyński test and baryon acoustic oscillations

The BAO scale provides a convenient standard ruler which can be detected both in the radial (z) and transverse directions (θ) leading to a determination of the quantity

$$F(z) \equiv \left| \frac{\delta z}{\delta \theta} \right| = \frac{(1+z) H(z) d_{_A}(z)}{c} = \frac{H(z) D(z)}{c} \tag{66}$$

related to the Alcock–Paczyński test[21] [130]. The BAO scale has now been detected at several redshifts in galaxy clustering statistics [131, 132] and the Lyman–α forest [133], and provide a promising geometric test of the expansion history.

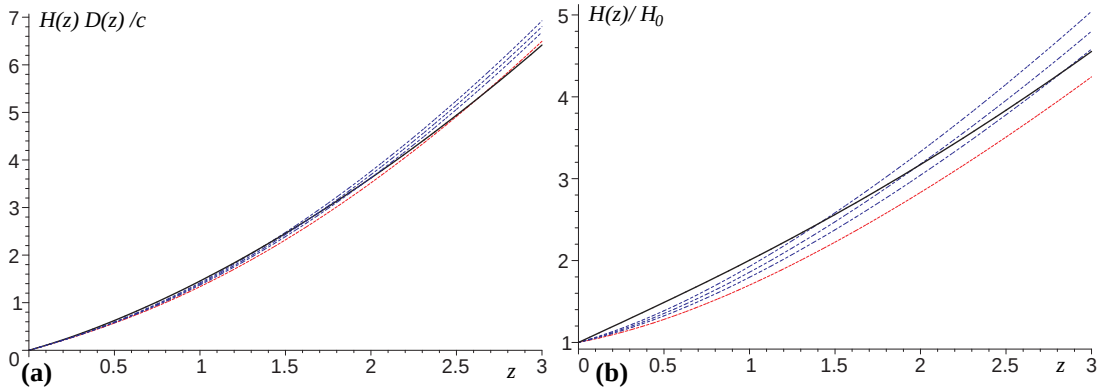

FIGURE 10. **(a)** $F(z) = c^{-1} H(z) D(z)$; **(b)** $H(z)/H_{_0}$. In each we display curves for the timescape model with $f_{\rm v0} = 0.695$ (solid line), and comparison spatially flat ΛCDM models (dashed lines): for the 3 values of $\Omega_{_{M0}}$ shown in Fig. 8, and also the value $\Omega_{_{M0}} = 0.27$ used in the fits of [131]-[133]. In both panels the ΛCDM curves are arranged from bottom to top by the values of $\Omega_{_{M0}} = 0.27, 0.3175, 0.35, 0.388$.

In Fig. 10 we show the test function $F = HD/c$ and also the function $H(z)/H_{_0}$ (with dressed Hubble parameter) for timescape and ΛCDM examples, over the range of redshifts tested to date [131]–[133]. In fact, at the effective redshifts tested in the WiggleZ survey, for $f_{\rm v0} = 0.695$ the timescape values $F(0.21) = 0.246$, $F(0.41) = 0.496$, $F(0.60) = 0.776$, $F(0.78) = 1.067$ all agree with the Alcock–Paczyński fits of this quantity in Table 1 of ref. [131], within uncertainties. While this is encouraging, the methods of analysis used for the BAO scale assume the standard model, both in applying Fourier space techniques, and in treating redshift space distortions. These aspects of the data analysis need to be revisited from first principles in the timescape model before we can be completely confident in using constraints from these tests.

From Fig. 10(a) we see that the expectations for $H(z)D(z)/c$ for the timescape and ΛCDM models are very close for most of the redshift range currently considered. A

[21] Alcock and Paczyński [130] originally defined their test statistic as $f_{\rm AP} = z^{-1} F(z)$. Since $D(z) \to 0$ as $z \to 0$, the original Alcock–Paczyński test function is actually the derivative $F'(z)$ in the limit $z \to 0$, rather than $F(z)$. As seen in Fig. 8 of ref. [16] this statistic has a greater power to discriminate between the timescape and ΛCDM models. However, taking a derivative with respect to z requires better quality data, and for the time being one is limited to testing quantities such as (66) or $D_{\rm V} = (zD^2 H^{-1})^{1/3}$.

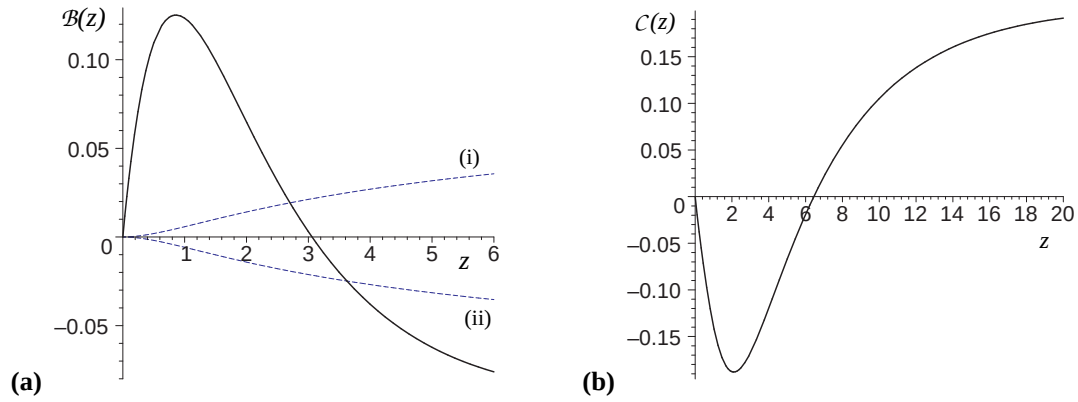

FIGURE 11. **(a)** The (in)homogeneity test function $\mathcal{B}(z) = [c^{-1}HD']^2 - 1$ is plotted for the timescape tracker solution with $f_{\rm v0} = 0.695$ (solid line), and compared to equivalent curves $\mathcal{B} = \Omega_{k0}(c^{-1}H_0D)^2$ for two ΛCDM models: **(i)** $\Omega_{M0} = 0.32$, $\Omega_{\Lambda 0} = 0.67$, $\Omega_{k0} = 0.01$; **(ii)** $\Omega_{M0} = 0.32$, $\Omega_{\Lambda 0} = 0.69$, $\Omega_{k0} = -0.01$. **(b)** The (in)homogeneity test function $\mathcal{C}(z)$ is plotted for the $f_{\rm v0} = 0.695$ tracker solution.

more discriminating test can in principle be obtained by dividing the curve of Fig. 10(a) by that of Fig. 8 to produce the quantity $H(z)/H_0$ shown in Fig. 10(b). The most notable feature is that the slope of $H(z)/H_0$ is less than in the ΛCDM cases, as is to be expected for a model whose (dressed) deceleration parameter varies more slowly than for ΛCDM. Two different measurements are required to produce this information, however, both the BAO measurement to determine $H(z)D(z)/c$, and luminosity distance measurements to determine $H_0D(z)/c$. In addition to examining the model–dependent issues in BAO measurements, it also necessitates sorting out the systematics of SNeIa that currently limit model comparison, as discussed in Sec. 6.1.

6.5. Test of (in)homogeneity

Clarkson, Bassett and Lu [134] have constructed a test statistic based on the observation that for homogeneous, isotropic models which obey the Friedmann equation, the present epoch curvature parameter, a constant, may be written as

$$\Omega_{k0} = \frac{[c^{-1}H(z)D'(z)]^2 - 1}{[c^{-1}H_0D(z)]^2} \tag{67}$$

for all z, irrespective of the dark energy model or any other model parameters. Consequently, taking a further derivative, the quantity

$$\mathcal{C}(z) \equiv 1 + c^{-2}H^2(DD'' - D'^2) + c^{-2}HH'DD' \tag{68}$$

must be zero for all redshifts for any FLRW geometry. A deviation of $\mathcal{C}(z)$ from zero, or of (67) from a constant value, would therefore mean that the assumption of FLRW evolution is violated.

The functions (67) and (68) are computed in ref. [16]. It is more feasible to fit (67) than which involves one derivative less of redshift. In Fig. 11 we show both $\mathcal{C}(z)$, and

also the function $\mathcal{B}(z) = [c^{-1}HD']^2 - 1$ from the numerator of (67) for the timescape model, as compared to two ΛCDM models with a small amount of spatial curvature. A spatially flat FLRW model would have $\mathcal{B}(z) \equiv 0$. The timescape $\mathcal{B}(z)$ function is easily distinguishable from the FLRW cases. However, this requires better quality data than is currently available. As noted in Sec. 6.4, present BAO data is able to constraint $H(z)D(z)$ but not yet $H(z)D'(z)$. Therefore, while the Clarkson, Bassett and Lu test [134] is a powerful one, it may be some time before it can be implemented.

6.6. Time drift of cosmological redshifts

As noted in Sec. 6.4, the combined measurements of $H_0 D(z)/c$ and $H(z)D(z)/c$ provide a means to determine $H(z)$ which at present is subject to model dependencies and many systematic uncertainties. A model independent determination of $H(z)$, which is also needed to determine the quantity $\mathcal{B}(z)$ in the (in)homogeneity test of Sec. 6.5, is provided by a measurement of the real time variation of the redshifts of distant sources over a long time period [135]–[137]. Although extremely challenging, such a measurement may be possible over a 20 year period by precision measurements of the Lyman-α forest in the redshift range $2 < z < 5$ with the next generation of Extremely Large Telescopes [138, 139].

In ref. [16] an analytic expression for $H_0^{-1}\frac{\mathrm{d}z}{\mathrm{d}\tau}$ is determined, the derivative being with respect to wall time for observers in galaxies. The resulting function is displayed in Fig. 12 for the timescape model with $f_{\mathrm{v}0} = 0.695$, and is compared to those of three spatially flat ΛCDM models. The timescape model curve is considerably flatter than those of the ΛCDM models. This is a consequence of the magnitude of the apparent acceleration being considerably smaller in the timescape model, as compared to the magnitude of the acceleration in ΛCDM models. For cosmologies with no apparent acceleration, $H_0^{-1}\frac{\mathrm{d}z}{\mathrm{d}\tau}$ is always negative. If there is cosmic acceleration at late epochs, real or apparent, then $H_0^{-1}\frac{\mathrm{d}z}{\mathrm{d}\tau}$ will become positive at low redshifts, though at a somewhat larger redshift than of the onset of (apparent) acceleration. For $f_{\mathrm{v}0} = 0.695$, $H_0^{-1}\frac{\mathrm{d}z}{\mathrm{d}\tau} > 0$ for $0 < z < 0.946$, but with a tiny amplitude compared to the ΛCDM models.

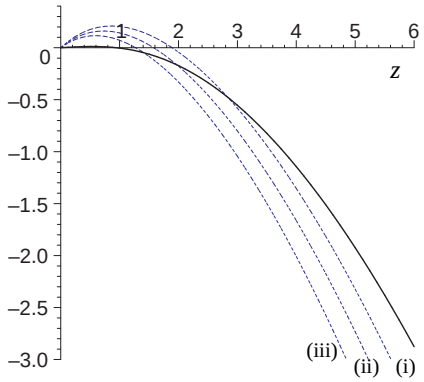

FIGURE 12. The function $H_0^{-1}\frac{\mathrm{d}z}{\mathrm{d}\tau}$ for the timescape model with $f_{\mathrm{v}0} = 0.695$ (solid line) is compared to $H_0^{-1}\frac{\mathrm{d}z}{\mathrm{d}\tau}$ for the three spatially flat ΛCDM models shown in Fig. 8 (dashed lines).

The very clear differences in redshift time drift for low redshifts $z \lesssim 2$ could lead to a decisive test of the timescape model versus ΛCDM models. Observationally, however, it is expected that measurements will be best determined for sources in the Lyman α forest in the range, $2 \lesssim z \lesssim 5$. At such redshifts the magnitude of the drift is somewhat more pronounced in the case of the ΛCDM models. For a source at $z = 4$, over a period of $\delta\tau = 10$ years we would have $\delta z = -7.2 \times 10^{-10}$ for the timescape model with $f_{\rm v0} = 0.695$ and $H_0 = 61.7 \,{\rm km\,s^{-1}\,Mpc^{-1}}$. By comparison, for a spatially flat ΛCDM model with $H_0 = 67.1 \,{\rm km\,s^{-1}\,Mpc^{-1}}$ and Ω_{M0} we have $\delta z = -9.3 \times 10^{-10}$ for the same source over 10 years. Different values of (H_0, Ω_{M0}) can produce degeneracies at particular redshifts. However, a large sample of sources over the whole range $2 \lesssim z \lesssim 5$ should be able to constrain the shape of the $H_0^{-1} \frac{{\rm d}z}{{\rm d}\tau}$ curve sufficiently to determine $H(z)$ in that range, and to distinguish the timescape and ΛCDM cosmologies.

7. VARIATION OF THE HUBBLE EXPANSION

Potentially the most interesting tests of the timescape model are those below the SHS, since here we should find variation of the Hubble expansion but with a scale–dependent amplitude constrained by the uniform quasilocal Hubble flow condition.

7.1. Problems and puzzles of bulk flows

Traditionally astronomers have almost always analysed the variation of the Hubble expansion in terms of *peculiar velocities*, namely as deviations from a linear Hubble law

$$v_{\rm pec} = cz - H_0 r \tag{69}$$

where r is an appropriate distance measure. Such a definition implicitly makes a strong assumption about spacetime geometry: on the scales of interest spatial curvature can be neglected and the redshift associated with the Hubble expansion can be treated in the manner of a recession velocity as in special relativity. A linear Hubble law is observed to hold out to redshifts $z \sim 0.1$, though on very small scales $z \lesssim 0.02$ below the SHS the Hubble flow enters into a 'nonlinear regime'.

For some decades astronomers have sought the scale on which peculiar velocities converge to the flow indicated by the CMB temperature dipole. The dipole is usually assumed to arise solely from a special relativistic boost, and in addition to the known motion of our Sun with respect to the barycentre of the Local Group (LG) of galaxies, this suggests that the LG itself is moving at $635 \pm 38 \,{\rm km\,s^{-1}}$ in a direction $(\ell, b) = (276.4^\circ, 29.3^\circ) \pm 3.2^\circ$ in galactic coordinates. This direction defines a *clustering dipole*, namely a direction in which it is expected we should find an overdensity which gravitationally attracts the LG, galaxies between the LG and the overdensity and galaxies on the other side of the overdensity.

There is no *a priori* reason why such Newtonian concepts of gravitational attraction should persist on very large scales on which space is expanding. Nonetheless, even though the very local Hubble flow on scales of tens of megaparsecs is nonlinear, a

linear Newtonian approximation is assumed to apply at larger scales, and the amplitude of the peculiar velocities of galaxies is estimated in a linearly perturbed FLRW model according to [140, 141]

$$\mathbf{v}(\mathbf{r}) = \frac{H_0 \Omega_{M0}^{0.55}}{4\pi} \int \mathrm{d}^3\mathbf{r}'\, \delta_m(\mathbf{r}')\, \frac{(\mathbf{r}' - \mathbf{r})}{|\mathbf{r}' - \mathbf{r}|^3} \tag{70}$$

where $\delta_m(\mathbf{r}) = (\rho - \bar{\rho})/\bar{\rho}$ is the density contrast.

The search for convergence of bulk flows within this framework has a three decade history summarized in refs. [142, 143]. Contrary to earlier investigations [144], Lavaux *et al*. [142] failed to find convergence in the 2MASS survey on scales up to $120\,h^{-1}$Mpc: less than half the amplitude was generated on scales $40\,h^{-1}$Mpc, and whereas most of the amplitude was generated within $120\,h^{-1}$Mpc the direction did not agree. Bilicki *et al*. [143] analysed a larger sample in the 2MASS survey using a different methodology and failed to find convergence within $150\,h^{-1}$Mpc. Some studies have found persistent bulk flows extending to very large scales [145]–[148], and their consistency with the ΛCDM model is much debated [149]–[151].

Recent attention has focused on the influence of the Shapley Concentration on our local motion, as this is a particularly dense concentration of galaxies in the clustering dipole direction. However, Shapley is at a distance of $138\,h^{-1}$Mpc, well beyond the SHS, and an influence at our location would represent an unusually large scale correlation. A very recent study [152] using SneIa fails to find a significant turnover in peculiar velocities on the other side of the Shapley Concentration, casting further doubt on the attractor model.

7.2. Model independent analysis of Hubble expansion variation

In general relativity it is well-known that every exact dust solution of the Einstein equations which is not spatially homogeneous and isotropic exhibits differential expansion of space. Furthermore, by the SEP the concept of a special relativistic boost applies only in a LIF in the neighbourhood of a point, and a general expansion of space cannot always be reduced to simple boosts. Consequently the conceptual framework we have just described in Sec. 7.1 represents an extrapolation of Newtonian concepts into a regime in which they cannot obviously be expected to be valid.

In the timescape scenario the greatest variations in spatial curvature occur below the SHS, and a spatially flat geometry cannot be assumed to apply at every scale. In recent work [153] we have analysed the variation of the Hubble expansion in a model independent manner, with no geometrical assumptions. We simply assumed that a linear average Hubble law exists in the leading approximation, and then determined the best-fit Hubble law in independent spherical shells, even in the regime of the nonlinear Hubble flow. The conceptual picture behind such averages is illustrated in Fig. 13.

Null geodesics (indicated by arrowed lines converging on a centre in Fig. 13) which traverse scales larger than the SHS experience an average expansion with cz/r defining a Hubble constant equal to that determined in spherical shells whose inner boundary is at least a few times larger than the largest typical nonlinear structures. Below the

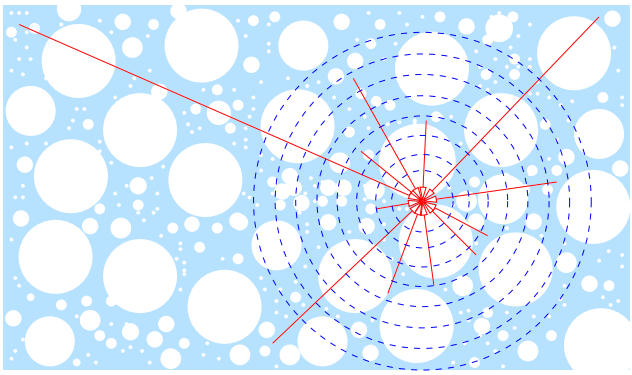

FIGURE 13. Schematic diagram of spherical averaging. The universe is described as ensemble of filaments, walls and voids: expanding regions of different density which have decelerated by different amounts and therefore experience different local expansion rates at the present epoch. If one averages cz/r in spherical shells (dotted lines) about a point then once the shells are a few times larger than the typical nonlinear structures [2]–[4], an average Hubble law with small statistical scatter is obtained, whereas there are considerable deviations for shells on scales comparable to the typical nonlinear structures.

SHS null geodesics which traverse a single void will experience a higher expansion rate than those that only traverse wall regions. We thus expect considerable variation in the average values of cz/r for sources in shells whose diameters are comparable to the largest typical nonlinear structures. Since the largest typical nonlinear structures are $\sim 30\,h^{-1}$Mpc diameter voids [2]–[3], and since these occupy a greater volume of space than walls and filaments, we expect that a spherical average of cz/r should in general produce larger than average values of the Hubble 'constant' on scales below the SHS. Furthermore, if the results of [31] are correct then an asymptotic average value of H_0 should emerge on $70\,h^{-1}$–$100\,h^{-1}$Mpc scales.

Finally, there is the question of the choice of cosmic rest frame. Since space is differentially expanding below the SHS (as measured by one set of clocks), the expansion law can be expected to differ from that of a spatially flat geometry with rigid expansion plus local boosts. In the timescape scenario the *finite infinity* scale defines the appropriate notion of a rest frame (the CIR), and for bound systems this should be a scale on which space is marginally expanding bounding a critical density volume. In addition to determining averages in the conventional CMB rest frame, we have also performed averages in the rest frames of the Local Group and the Local Sheet[22] (LS) [154].

In ref. [153] we analysed variation of the Hubble flow in the COMPOSITE sample of 4,534 galaxies compiled by Watkins, Feldman and Hudson [145, 146]. Spherical averages were computed in independent shells[23] with a minimum width of $12.5\,h^{-1}$Mpc.

---

[22] Since our galaxy is in a thin filamentary sheet in a local environment dominated by voids [154], the finite infinity scale should be relatively near. For rich clusters of galaxies the scale is larger.

[23] In earlier work, Li and Schwarz [155] performed a similar analysis of a subset of 54 distances from the Hubble Space Telescope (HST) Key project data, in the CMB rest frame only. With a very small sample they divided it into an inner and outer shell, with a moving boundary, producing a correlated average.

We minimized the sum $\chi^2 = \sum_i \left[\sigma_i^{-1}(r_i - cz_i/H)\right]^2$ with respect to H, where z_i, r_i and σ_i denote individual redshifts, distances and distance uncertainties (in units h^{-1}Mpc) respectively. This leads to a value of the Hubble constant in the sth shell,

$$H_s = \left(\sum_{i=1}^{N_s} \frac{(cz_i)^2}{\sigma_i^2}\right)\left(\sum_{i=1}^{N_s} \frac{cz_i r_i}{\sigma_i^2}\right)^{-1} . \tag{71}$$

Results for the fractional variation, $\delta H_s = \left(H_s - \bar{H}_0\right)/\bar{H}_0$, are plotted in Fig. 14 in the CMB and LG frames. Here $\bar{H}_0$ is the asymptotic value of the Hubble constant, determined from all the data in the sample beyond $r > 156.25\,h^{-1}$Mpc. Results in the LS frame values are very similar to the LG frame.

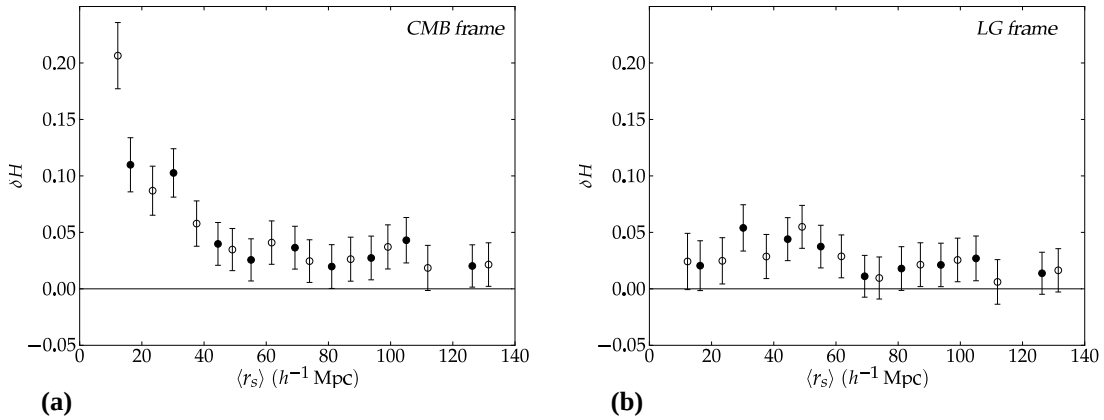

FIGURE 14. Fractional variation in the Hubble flow $\delta H_s = \left(H_s - \bar{H}_0\right)/\bar{H}_0$ in spherical shells as a function of weighted mean shell distance: **(a)** CMB frame; **(b)** LG frame. In each case the filled data points represent one choice of shells boundaries, and the open data points a second choice of shell boundaries. Each filled (open) data point is thus correlated to the two nearest neighbour open (filled) data points.

We see that the spherically averaged Hubble law is significantly more uniform in the LG frame than in the CMB frame. In the inner shells the Bayesian evidence in favour of the LG frame expansion being more uniform is very very strong with $\ln B > 10$ [153]. If the cosmic rest frame is defined as the one in which the Hubble expansion is most uniform, with minimal statistical variations, then from our vantage point the LG frame is much closer to having this character. Such a result is completely unexpected and surprising from the viewpoint of the standard cosmology, but does accord with the expectation of the timescape scenario that the local finite infinity scale should define the standard of rest for observers within a bound system. The frame of minimum Hubble expansion variance still remains to be determined, and this may still differ somewhat from the LG frame.

As discussed in ref. [153], if one performs a random boost on each data point, it involves replacing $cz_i \to cz_i' = cz_i + v\cos\phi_i$, where ϕ_i is the angle on the sky between the data point and the boost direction. In a dataset with uniform sky coverage, terms linear in the boost velocity will be roughly self-canceling inside the sums in (71), leaving a

leading order average difference

$$H_s' - H_s \sim \frac{v^2}{2H_0\langle r_i^2\rangle}\,. \tag{72}$$

The differences between panels (a) and (b) in Fig. 14 do indeed appear to have this character. This suggests that the persistent large scale bulk flows seen in the standard peculiar velocity framework may arise largely as a systematic error from choosing a cosmic rest frame which has a significant boost with respect to the frame in which statistical variations of the Hubble expansion are minimal.

An exception to the rule that $|\delta H_s|$ is smaller in the LG frame than in the CMB frame does occur for shells roughly in the range $40\,h^{-1} \lesssim r \lesssim 60\,h^{-1}$Mpc. It turns out that there is also a LG frame dipole associated with structures in this range. In ref. [153] in addition to studying radial spherical variations we also investigated angular variations by adapting a Gaussian window averaging method of McClure and Dyer [156]. This established that a dipole is the strongest angular multipole feature in both frames, but particularly in the LG frame, until one reaches distances $r \gtrsim 90\,h^{-1}$Mpc. We then fitted a simple dipole Hubble law

$$\frac{cz}{r} = H_d + \beta\cos\phi\,, \tag{73}$$

in the same independent spherical shells used for the spherical averages. This gave a dipole amplitude, β, shown in Fig. 15.

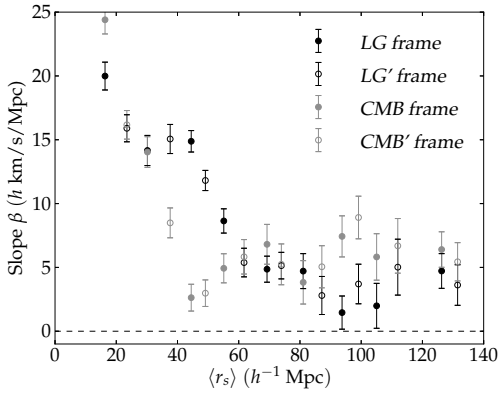

FIGURE 15. The slope β of the linear dipole relation $cz/r = H_d + \beta\cos\phi$, plotted in the same shells as Fig. 14 [153] in the CMB and LG rest frames.

The magnitudes of the dipoles in the two frames coincide in the shell with mean radius $\bar{r} = 30.2\,h^{-1}$Mpc, and also in the shell with $\bar{r} = 61.7\,h^{-1}$Mpc, but the dipoles exhibit very different behaviour for the shells in between. In particular, the CMB frame dipole magnitude reaches a minimum of $\beta = (2.6 \pm 0.6)h\,\mathrm{km\,s^{-1}\,Mpc^{-1}}$ (close to zero) at $\bar{r} = 44.5\,h^{-1}$Mpc, whereas for the LG frame $\beta = (14.9 \pm 0.8)h\,\mathrm{km\,s^{-1}\,Mpc^{-1}}$ in the same shell. The CMB frame dipole then increases while the LG frame dipole decreases. The dipole directions for independent shells within each frame are strongly consistent in the range $37.5\,h^{-1} \leq r \leq 62.5\,h^{-1}$Mpc. Beyond $\bar{r} = 61.7\,h^{-1}$Mpc, the CMB frame dipole

maintains statistically significant residual levels, while the LG frame dipole drops to a level statistically consistent with zero around $90\,h^{-1}$–$100\,h^{-1}$Mpc[24].

It therefore appears that the boost to the CMB frame is largely compensating for the effect of structures in the range $37.5\,h^{-1} \leq r \leq 62.5\,h^{-1}$Mpc, which are also responsible for monopole variations of the Hubble 'constant' in the LG frame shown in Fig. 14. The results are consistent with a foreground density gradient producing an anisotropy in the distance–redshift relation which is almost, but not exactly, of the same nature as the Doppler shift produced by a Lorentz boost. Rather than thinking purely about overdensities as in the attractor model, what is important below the SHS are the peculiar foregrounds created by voids as well as by superclusters. Those directions in which void–filled foregrounds are opposed to wall regions on the opposite side of the sky will lead to the strongest density gradients. Relevant structures are identified in Sec. III C of ref. [153].

7.3. Origin of the CMB dipole

It was further established in ref. [153] that the Gaussian window averaged sky map of angular Hubble flow variation in the LG frame has a correlation coefficient of -0.92 with the map that would be produced by the residual CMB temperature dipole in the LG rest frame. The correlation coefficient is insensitive to the choice of the Gaussian window smoothing angle in the range $15^\circ < \sigma_\theta < 40^\circ$.

The strong correlation of the two sky maps is consistent with the hypothesis that the CMB temperature dipole is only partly due to a Lorentz boost. The portion usually attributed to the motion of the LG might be largely due to the differential expansion of space produced by peculiar foregrounds below the SHS. In the LG frame the residual temperature dipole is $\delta T = \pm(5.77 \pm 0.36)$ mK. For the ΛCDM model with Planck best-fit parameters, this would be produced by an anisotropy $\delta D = \mp(0.30 \pm 0.02)\,h^{-1}$Mpc in the distance to the surface of last scattering. The value for the timescape model is essentially the same. If produced by the differential expansion of foreground structures within a mean distance of $60\,h^{-1}$Mpc, this amounts to a 0.5% anisotropy on these scales, which is entirely plausible[25].

There is differential expansion of space below the SHS at all locations, of a magnitude bounded by the growth of structure from the initial perturbations at the surface of last scattering. CMB photons which traverse large distances see an average of all of these variations, producing an average distance to the last scattering surface. However, the last stretch of the journey produces slight differences that depend on peculiar density foregrounds. The same small residual anisotropies will apply to all cosmic distance measurements on scales much greater than the SHS, but at a level smaller than the

[24] Beyond this scale the quadrupole becomes as strong as the dipole, and one needs to fit higher multipoles. There is a hint of a small feature in the LG frame at scale corresponding to one BAO distance beyond the nearest wall. However, significantly more data is required in the outer shells to verify this.

[25] As is discussed in Sec. VI A of ref. [153] a multipole decomposition of the Hubble expansion should be developed, in spherical shells, to determine whether the dipole converges to the required amplitude.

uncertainties in many large scale measurements.

Although it might generally be expected that a differential expansion of space would produce higher order multipole CMB anisotropies of a magnitude comparable to the CMB dipole, these are in fact highly suppressed for off–centre observers in voids [157], which represent a good first approximation for our actual local environment [154]. Ray tracing in a simple LTB void with parameters matched to the LG frame Hubble dipole of Fig. 15 gives a CMB quadrupole/dipole ratio of less than 0.1% [153]. Using the Szekeres models [158, 159] one can perform ray tracing through exact solution geometries which more closely mimic our peculiar foregrounds; while a higher quadrupole/dipole CMB ratio of order 1% is found, this is still observationally viable [160].

The suggestion that a large fraction of the CMB dipole is not purely due to a boost is, of course, a radical departure for observational cosmology. However, a number of potential anomalies have been observed in the large angles multipoles of the CMB anisotropy spectrum for a decade now, and their significance has increased with the release of the Planck data [161]. A study by Freeman *et al*. [162] found that of several possible systematic errors, a 1–2% error in the CMB dipole subtraction stood out as the one possible effect which could potentially resolve the power asymmetry anomaly.

As is discussed in ref. [153] a nonkinematic contribution to the foreground Hubble expansion may also explain why attempts to measure the effects of aberration and frequency modulation in the Doppler boosting of the CMB spectrum yield a boost direction which moves across the sky when only large angle multipoles are considered [163]. Aberration and frequency modulation can also be readily tested in the radio spectrum. Rubart and Schwarz [164] have recently found that the assumption of a kinematic origin for the cosmic radio galaxy dipole is inconsistent at the 99.5% confidence level, using the NRAO VLA Sky Survey data. The direction of the radio dipole is consistent with that of the Hubble variance dipole we find in the LG frame.

8. CONCLUSION

Observations over the last few decades have revealed a universe much more complex, varied and interesting than had been previously imagined. The observations are at present well in advance of our theoretical understanding. The phenomenon of apparent cosmic acceleration demands that we think more deeply about one of the central unsolved problems of general relativity: the nature of gravitational mass–energy, which cannot be localized on account of the equivalence principle. The standard ΛCDM model adds cold dark matter to make gravity stronger at some scales and then adds dark energy to make gravity weaker at larger scales, while keeping space rigidly expanding. Both phenomena may be indicative of a renormalization of the notion of gravitational mass in a hierarchy of nonrigid spacetime structures.

The timescape scenario is a from–first–principles attempt to come to grips with the essential physics of the fitting problem [10, 11], and to specify a physically viable interpretation of the Buchert averaging scheme [48, 49, 76] without a smooth “dark energy”. A phenomenological model has been developed [13, 16, 103], which had remained observationally viable over the six years since its conception [13]. Much work remains to be done. In particular, while the tests of Secs. 6.1–6.6 give a means

of comparing average cosmological quantities with those of the ΛCDM model, the most exciting developments are to be made by considering physics below the SSH. This may also inform the development of tests related to the average growth of structure.

It is below the SSH, where the structures are most inhomogeneous, that the most interesting differences between the timescape scenario and the standard cosmology are to be found. In the ΛCDM model spacetime is spatially flat on these scales, while in the timescape scenario its spatial curvature varies greatly. A rigorous mathematical description of the statistical geometry on these scales remains to be determined. However, to develop such a description I believe we should not be guided simply by mathematical elegance but by physical principles and observations.

The simple idea that the finite infinity scale should define the cosmic rest frame for bound system observers led to the idea of testing the Hubble expansion variation in the LG and LS frames, as well as in the CMB frame, with a result that was much more definitive than we ourselves anticipated [153]. Since the analysis of Sec. 7 is model–independent it is not a direct verification of the timescape scenario; but it is consistent with the timescape model and it is extremely hard to reconcile with the standard cosmology. As discussed in ref. [153], a change to our understanding of the local Hubble expansion variation and its effect on the CMB dipole may have some impact on many different aspects of observational cosmology, including not only CMB anomalies but also SneIa systematics and the calibration of the distance scale.

ACKNOWLEDGMENTS

This work was supported by the Marsden fund of the Royal Society of New Zealand. I thank Krzysztof Bolejko, Teppo Mattsson, Ahsan Nazer, Peter Smale, Nezihe Uzun and Rick Watkins for helpful discussions and correspondence. I also wish to thank Mario Novello and Santiago Perez Bergliaffa for their support and for organizing a very memorable cosmology school.

REFERENCES

1. P. A. R. Ade, N. Aghanim, C. Armitage-Caplan, *et al.*, *Astron. Astrophys.* **571**, A16 (2014).
2. F. Hoyle and M. S. Vogeley, *Astrophys. J.* **566**, 641 (2002).
3. F. Hoyle and M. S. Vogeley, *Astrophys. J.* **607**, 751 (2004).
4. D. C. Pan, M. S. Vogeley, F. Hoyle, Y. Y. Choi, and C. Park, *Mon. Not. R. Astr. Soc.* **421**, 926 (2012).
5. A. V. Tikhonov and I. D. Karachentsev, *Astrophys. J.* **653** (2006) 969.
6. J. E. Forero-Romero, Y. Hoffman, S. Gottloeber, A. Klypin and G. Yepes, *Mon. Not. R. Astr. Soc.* **396**, 1815 (2009).
7. J. R. Gott, M. Juric, D. Schlegel, F. Hoyle, M. Vogeley, M. Tegmark, N. Bahcall and J. Brinkmann, *Astrophys. J.* **624**, 463 (2005).
8. A. Einstein, Sitzungsber. Preuss. Akad. Wiss., 142 (1917). [English translation in *"The collected papers of Albert Einstein. Vol.* **6***"*, (Princeton University Press, 1997) pp. 421–432]
9. A. Einstein and E. G. Straus, *Rev. Mod. Phys.* **17**, 120 (1945); Err. **18**, 148 (1946).
10. G. F. R. Ellis, in B. Bertotti, F. de Felice and A. Pascolini (eds), *General Relativity and Gravitation*, (Reidel, Dordrecht, 1984) pp. 215–288.
11. G. F. R. Ellis and W. Stoeger, *Class. Quantum Grav.* **4**, 1697 (1987).
12. H. Bondi, *Cosmology*, (Cambridge University Press, 1961)

13. D. L. Wiltshire, *New J. Phys.* **9**, 377 (2007).
14. D. L. Wiltshire, *Phys. Rev. Lett.* **99**, 251101 (2007).
15. D. L. Wiltshire, *Phys. Rev.* D **78**, 084032 (2008).
16. D. L. Wiltshire, *Phys. Rev.* D **80**, 123512 (2009).
17. M. Milgrom, *Astrophys. J.* **270**, 365 (1983).
18. R. H. Sanders and S. S. McGaugh, Ann. Rev. *Astron. Astrophys.* **40**, 263 (2002).
19. F. I. Cooperstock and S. Tieu, *Mod. Phys. Lett. A* **21**, 2133 (2006).
20. F. I. Cooperstock and S. Tieu, *Int. J. Mod. Phys.* A **22**, 2293 (2007).
21. H. Balasin and D. Grumiller, *Int. J. Mod. Phys.* D **17**, 475 (2008).
22. A. Rakić and D. J. Schwarz, *PoS* **IDM2008**, 096 (2008) [arXiv:0811.1478].
23. G. Lemaître, *Ann. Soc. Sci. Bruxelles* A **53**, 51 (1933) [*Gen. Relativ. Grav.* **29**, 641 (1997)].
24. R. C. Tolman, Proc. Nat. Acad. Sci. **20**, 169 (1934);
25. H. Bondi, *Mon. Not. R. Astr. Soc.* **107**, 410 (1947).
26. K. Bolejko, A. Krasiński and C. Hellaby, *Mon. Not. R. Astr. Soc.* **362**, 213 (2005).
27. G. F. R. Ellis and W. Stoeger, *Mon. Not. R. Astr. Soc.* **398**, 1527 (2009).
28. R. G. Clowes, K. A. Harris, S. Raghunathan, *et al*., *Mon. Not. R. Astr. Soc.* **429**, 2910 (2013).
29. D. W. Hogg, D. J. Eisenstein, M. R. Blanton, N. A. Bahcall, J. Brinkmann, J. E. Gunn, and D. P. Schneider, *Astrophys. J.* **624**, 54 (2005).
30. F. Sylos Labini, N. L. Vasilyev, L. Pietronero, and Y. V. Baryshev, Europhys. Lett. **86**, 49001 (2009).
31. M. Scrimgeour, T. Davis, C. Blake, *et al*., *Mon. Not. R. Astr. Soc.* **425**, 116 (2012).
32. D. J. Eisenstein, I. Zehavi, D. W. Hogg, *et al*., *Astrophys. J.* **633** 560, (2005).
33. S. Cole, W. J. Percival, J. A. Peacock, *et al*., *Mon. Not. R. Astr. Soc.* **362**, 505 (2005).
34. F. Sylos Labini, M. Montuori and L. Pietronero, Phys. Rep. **293**, 61 (1998).
35. Y. Baryshev, AIP Conf. Proc. **822**, 23 (2006).
36. A. D. Chernin, I. D. Karachentsev, M. J. Valtonen, V. P. Dolgachev, L. M. Domozhilova and D.I. Makarov, *Astron. Astrophys.* **415**, 19 (2004).
37. A. Sandage, G.A. Tammann and E. Hardy, *Astrophys. J.* **172**, 253 (1972).
38. G. de Vaucouleurs, Science **167**, 1203 (1970).
39. M. Axenides and L. Perivolaropoulos, *Phys. Rev.* D **65**, 127301 (2002).
40. M. Korzyński, *Class. Quantum Grav.* **27**, 105015 (2010).
41. R. Arnowitt, S. Deser and C. W. Misner, in L. Witten (ed), *Gravitation: An introduction to current research*, (Wiley, New York, 1962) pp. 227–265.
42. R. W. Lindquist and J. A. Wheeler, *Rev. Mod. Phys.* **29**, 432 (1957); Err. **31**, 839 (1959).
43. T. Clifton and P. G. Ferreira, *Phys. Rev.* D **80**, 103503 (2009).
44. T. Clifton, *Class. Quantum Grav.* **28**, 164011 (2011)
45. J. P. Uzan, G. F. R. Ellis and J. Larena, *Gen. Relativ. Grav.* **43**, 191 (2011).
46. T. Clifton, P. G. Ferreira and K. O'Donnell, *Phys. Rev.* D **85**, 023502 (2012).
47. D. L. Wiltshire, *Class. Quantum Grav.* **28**, 164006 (2011).
48. T. Buchert, *Gen. Relativ. Grav.* **40**, 467 (2008).
49. T. Buchert, *Class. Quantum Grav.* **28**, 164007 (2011).
50. R. J. van den Hoogen, in T. Damour, R. T. Jantzen and R. Ruffini (eds), *Proceedings of the 12th Marcel Grossmann Meeting on General Relativity*, (World Scientific, Singapore, 2012) pp. 578-589.
51. C. Clarkson, G. F. R. Ellis, J. Larena and O. Umeh, *Rept. Prog. Phys.* **74**, 112901 (2011).
52. R. M. Zalaletdinov, *Gen. Relativ. Grav.* **24**, 1015 (1992).
53. R. M. Zalaletdinov, *Gen. Relativ. Grav.* **25**, 673 (1993).
54. R. M. Zalaletdinov, *Bull. Astron. Soc. India* **25**, 401 (1997).
55. P. Fleury, H. Dupuy and J. P. Uzan, *Phys. Rev.* D **87**, 123526 (2013).
56. P. Fleury, H. Dupuy and J. P. Uzan, *Phys. Rev. Lett.* **111**, 091302 (2013).
57. V. Marra and A. Notari, *Class. Quantum Grav.* **28**, 164004 (2011).
58. E. W. Kolb, *Class. Quantum Grav.* **28**, 164009 (2011).
59. P. J. E. Peebles, *AIP Conf. Proc.* **1241**, 175 (2010).
60. M. Carfora and K. Piotrkowska, *Phys. Rev.* D **52**, 4393 (1995).
61. M. Carfora and A. Marzuoli, *Phys. Rev. Lett.* **53**, 2445 (1984).
62. T. Buchert and M. Carfora, *Class. Quantum Grav.* **19**, 6109 (2002).
63. M. Carfora and T. Buchert, in *"Waves and Stability in Continuous Media"* eds. M. Nanganaro, M. Ronaco and R. Sionero, (World Scientific, Singapore, 2008) pp. 118-127 [arXiv:0801.0553].

64. C. Anastopoulos, *Phys. Rev.* D **79**, 084029 (2009).
65. J. Brannlund, R. J. van den Hoogen and A. A. Coley, *Int. J. Mod. Phys.* D **19**, 1915 (2010).
66. M. Reiris, *Class. Quantum Grav.* **25**, 085001 (2008).
67. M. Reiris, *Gen. Relativ. Grav.* **41**, 1083 (2009).
68. M. Mars and R. M. Zalaletdinov, *J. Math. Phys.* **38**, 4741 (1997).
69. A. Paranjape and T. P. Singh, *Phys. Rev.* D **76**, 044006 (2007).
70. A. A. Coley, N. Pelavas and R. M. Zalaletdinov, *Phys. Rev. Lett.* **95**, 151102 (2005).
71. A. Paranjape, *Phys. Rev.* D **78**, 063522 (2008).
72. A. Paranjape and T. P. Singh, *Phys. Rev. Lett.* **101**, 181101 (2008).
73. R. J. van den Hoogen, *J. Math. Phys.* **50**, 082503 (2009).
74. T. Buchert and J. Ehlers, *Astron. Astrophys.* **320**, 1 (1997).
75. J. Ehlers and T. Buchert, *Gen. Relativ. Grav.* **29**, 733 (1997).
76. T. Buchert, *Gen. Relativ. Grav.* **32**, 105 (2000).
77. T. Buchert, *Gen. Relativ. Grav.* **33**, 1381 (2001).
78. J. Behrend, I. A. Brown and G. Robbers, *J. Cosmol. Astropart. Phys.* 01 (2008) 013.
79. J. Larena, *Phys. Rev.* D **79**, 084006 (2009).
80. I. A. Brown, J. Behrend and K. A. Malik, *J. Cosmol. Astropart. Phys.* 11 (2009) 027.
81. C. Clarkson, K. Ananda and J. Larena, *Phys. Rev.* D **80**, 083525 (2009).
82. M. Gasperini, G. Marozzi and G. Veneziano, *J. Cosmol. Astropart. Phys.* 02 (2010) 009.
83. S. Räsänen, *J. Cosmol. Astropart. Phys.* 03 (2010) 018.
84. H. Russ, M. H. Soffel, M. Kasai and G. Börner, *Phys. Rev.* D **56**, 2044 (1997).
85. J. M. Bardeen, *Phys. Rev.* D **22**, 1882 (1980).
86. J. Bičák, J. Katz and D. Lynden-Bell, *Phys. Rev.* D **76**, 063501 (2007).
87. L. Smarr and J. W. York, *Phys. Rev.* D **17**, 2529 (1978).
88. L. B. Szabados, *Liv. Rev. Rel.* **7**, 4 (2004).
89. A. Komar *Phys. Rev.* **113**, 934 (1959).
90. M. Heusler, *"Black hole uniqueness theorems"*, (Cambridge University Press, 1996) pp. 14–17.
91. J. D. Brown and J. W. York, *Phys. Rev.* D **47**, 1407 (1993).
92. R. J. Epp, *Phys. Rev.* D **62**, 124018 (2000).
93. C. M. Chen, J. L. Liu and J. M. Nester, *Mod. Phys. Lett. A* **22**, 2039 (2007).
94. J. M. Nester, L. L. So and T. Vargas, *Phys. Rev.* D **78**, 044035 (2008).
95. M. F. Wu, C. M. Chen, J. L. Liu and J. M. Nester, *Phys. Lett. A* **374**, 3599 (2010).
96. R. A. Sussman, *Phys. Rev.* D **79**, 025009 (2009).
97. M. M. Afshar, *Class. Quantum Grav.* **26**, 225005 (2009).[arXiv:0903.3982]
98. T. Buchert and M. Carfora, *Phys. Rev. Lett.* **90**, 031101 (2003).
99. S. Viaggiu, 2012 *Class. Quantum Grav.* **29** 035016
100. S. Viaggiu and M. Montuori, *Int. J. Mod. Phys.* D **22**, 1350065 (2013).
101. T. Buchert and M. Carfora, *Class. Quantum Grav.* **25**, 195001 (2008).
102. A. Wiegand and T. Buchert, *Phys. Rev.* D **82**, 023523 (2010).
103. J. A. G. Duley, M. A. Nazer, and D. L. Wiltshire, *Class. Quantum Grav.* **30**, 175006 (2013).
104. S. S. McGaugh, *Astrophys. J.* **683**, 137 (2008).
105. B. M. Leith, S. C. C. Ng and D. L. Wiltshire, *Astrophys. J.* **672**, L91 (2008).
106. P. R. Smale and D. L. Wiltshire, *Mon. Not. R. Astr. Soc.* **413**, 367 (2011).
107. P. R. Smale, *Mon. Not. R. Astr. Soc.* **418**, 2779 (2011).
108. S. Jha, A. G. Riess and R. P. Kirshner, *Astrophys. J.* **659**, 122 (2007).
109. J. Guy, P. Astier, S. Nobili, N. Regnault and R. Pain, *Astron. Astrophys.* **443**, 781 (2005).
110. J. Guy, P. Astier, S. Baumont, *et al*., *Astron. Astrophys.* **466**, 11 (2007).
111. D. L. Wiltshire, in J. A. Auping (ed), *Proceedings of the International Conference on Two Cosmological Models*, (Plaza y Valdés, Mexico City, 2012) pp. 361-384 [arXiv:1102.2045].
112. D. L. Wiltshire, in T. Damour, R. T. Jantzen and R. Ruffini (eds), *Proceedings of the 12th Marcel Grossmann Meeting on General Relativity*, (World Scientific, Singapore, 2012) pp. 434-452.
113. A. G. Riess, L.-G. Strolger, S. Casertano, *et al*., *Astrophys. J.* **659**, 98 (2007).
114. R. Kessler, A. Becker, D. Cinabro, *et al*., *Astrophys. J. Suppl.* **185**, 32 (2009).
115. M. Hicken, W. M. Wood-Vasey, S. Blondin, P. Challis, S. Jha, P. L. Kelly, A. Rest and R. P. Kirshner, *Astrophys. J.* **700**, 1097 (2009).
116. B. E. Schaefer, *Astrophys. J.* **660**, 16 (2007).

117. N. Liang, W. K. Xiao, Y. Liu and S. N. Zhang, *Astrophys. J.* **685**, 354 (2008).
118. L. Amati, C. Guidorzi, F. Frontera, M. Della Valle, F. Finelli, R. Landi and E. Montanari, *Mon. Not. R. Astr. Soc.* **391**, 577 (2008).
119. L.Amati and M. Della Valle, *Int. J. Mod. Phys.* D **22**, 1330028 (2013).
120. R. H. Cyburt, B. D. Fields and K. A. Olive, *J. Cosmol. Astropart. Phys.* 11 (2008) 012.
121. D. D. Tytler, J. M. O'Meara, N. Suzuki and D. Lubin, Phys. Scripta T **85**, 12 (2000).
122. G. Steigman, *Int. J. Mod. Phys.* E **15**, 1 (2006).
123. B. F. Roukema, J. J. Ostrowski and T. Buchert, *J. Cosmol. Astropart. Phys.* 10 (2013) 043.
124. G. B. Zhao and X. Zhang, *Phys. Rev.* D **81**, 043518 (2010).
125. P. Serra, A. Cooray, D. E. Holz, A. Melchiorri, S. Pandolfi and D. Sarkar, *Phys. Rev.* D **80**, 121302 (2009).
126. J. A. Gu, C. W. Chen and P. Chen, *New J. Phys.* **11**, 073029 (2009).
127. C. Zunckel and C. Clarkson, *Phys. Rev. Lett.* **101**, 181301 (2008).
128. V. Sahni, A. Shafieloo and A. A. Starobinsky, *Phys. Rev.* D **78**, 103502 (2008).
129. A. Shafieloo, V. Sahni and A. A. Starobinsky, *Phys. Rev.* D **80**, 101301 (2009).
130. C. Alcock and B. Paczyński, *Nature* **281**, 358 (1979).
131. C. Blake, K. Glazebrook, T. Davis, *et al*., *Mon. Not. R. Astr. Soc.* **418**, 1725 (2011).
132. L. Anderson, E. Aubourg, S. Bailey, *et al*., *Mon. Not. R. Astr. Soc.* **427**, 343 (2013).
133. A. Slosar, V. Irsic, D. Kirkby, *et al*., *J. Cosmol. Astropart. Phys.* 04 (2013) 026.
134. C. Clarkson, B. Bassett and T. C. Lu, *Phys. Rev. Lett.* **101**, 011301 (2008).
135. A. Sandage, *Astrophys. J.* **136**, 319 (1962).
136. G. C. McVittie, *Astrophys. J.* **136**, 334 (1962).
137. A. Loeb, *Astrophys. J.* **499**, L111 (1998).
138. P. S. Corasaniti, D. Huterer and A. Melchiorri, *Phys. Rev.* D **75**, 062001 (2007).
139. J. Liske, A. Grazian, E. Vanzella, *et al*., *Mon. Not. R. Astr. Soc.* **386**, 1192 (2008).
140. P. J. E. Peebles, *Principles of Physical Cosmology*, (Princeton University Press, 1993).
141. E. V. Linder, *Phys. Rev.* D **72**, 043529 (2005).
142. G. Lavaux, R. B. Tully, R. Mohayaee, and S. Colombi, *Astrophys. J.* **709**, 483 (2010).
143. M. Bilicki, M. Chodorowski, G. A. Mamon, and T. Jarrett, *Astrophys. J.* **741**, 31 (2011).
144. P. Erdoğdu, O. Lahav, J. P. Huchra, *et al*., *Mon. Not. R. Astr. Soc.* **373**, 45 (2006).
145. R. Watkins, H.A. Feldman, and M.J. Hudson, *Mon. Not. R. Astr. Soc.* **392**, 743 (2009).
146. H.A. Feldman, R. Watkins, and M.J. Hudson, *Mon. Not. R. Astr. Soc.* **407**, 2328 (2010).
147. A. Kashlinsky, F. Atrio-Barandela, D. Kocevski, and H. Ebeling, *Astrophys. J.* **686**, L49 (2008).
148. A. Kashlinsky, F. Atrio-Barandela, H. Ebeling, A. Edge, and D. Kocevski, *Astrophys. J.* **712**, L81 (2010).
149. A. Nusser and M. Davis, *Astrophys. J.* **736**, 93 (2011).
150. Y.Z. Ma and D. Scott, *Mon. Not. R. Astr. Soc.* **428**, 2017 (2013).
151. S.J. Turnbull, M.J. Hudson, H.A. Feldman, M. Hicken, R.P. Kirshner, and R. Watkins, *Mon. Not. R. Astr. Soc.* **420**, 447 (2012).
152. U. Feindt, M. Kerschhaggl, M. Kowalski, *et al*., *Astron. Astrophys.* **560**, A90 (2013).
153. D. L. Wiltshire, P. R. Smale, T. Mattsson and R. Watkins, *Phys. Rev.* D **88**, 083529 (2013).
154. R.B. Tully, E.J. Shaya, I.D. Karachentsev, H. Courtois, D.D. Kocevski, L. Rizzi and A. Peel, *Astrophys. J.* **676**, 184 (2008).
155. N. Li and D.J. Schwarz, *Phys. Rev.* D **78**, 083531 (2008).
156. M.L. McClure and C.C. Dyer, New Astron. **12**, 533 (2007).
157. H. Alnes and M. Amarzguioui, *Phys. Rev.* D **74**, 103520 (2006).
158. P. Szekeres, Commun. Math. Phys. **41**, 55 (1975).
159. K. Bolejko and J.S.B. Wyithe, *J. Cosmol. Astropart. Phys.* 02 (2009) 020.
160. K. Bolejko, M.A. Nazer and D.L. Wiltshire, in preparation.
161. P. A. R. Ade, N. Aghanim, C. Armitage-Caplan, *et al*., *Astron. Astrophys.* **571**, A23 (2014).
162. P.E. Freeman, C.R. Genovese, C.J. Miller, R.C. Nichol, and L. Wasserman, *Astrophys. J.* **638**, 1 (2006).
163. N. Aghanim, C. Armitage-Caplan, M. Arnaud, *et al*., *Astron. Astrophys.* **571**, A27 (2014).
164. M. Rubart and D.J. Schwarz, *Astron. Astrophys.* **555**, A117 (2013).